

Chapter 3

Study of Commercial Lamp Phosphors

The commercial lamp phosphors were obtained from the industry in small quantities. The samples are from reputed lamp manufacturers like Philips (Holland, India) General Electric (USA), Osram, Cona and Solichem. However the samples have been coded as P-1, P-2, ----, P-6 to maintain anonymity. Lamps using these phosphors were made at the manufacturing site of a reputed company. The data on the lumen output and colour coordinates for five lamps were studied, for each category of phosphor. The quantum efficiency, fluorescence spectra, thermoluminescence glow curves and their spectrum were recorded using standard equipments described in Chapter 2. For better understanding of the trapping sites/centres, the EPR spectra was taken. The characterisation of the phosphors was done using XRD technique.

Characterisation of Commercial Phosphors :

The six samples of commercial lamp phosphors were characterised using X-ray diffraction technique. The XRD pattern was recorded on a PHILIPS PW-1840 machine having a 2θ range from 0 to 120° . A 3 kilowatt lamp was used for the copper k_α line with 1.542\AA . The line selection is done using a $130\mu\text{m}$ thick nickel filter. No monochromator is used for the purpose. The intensity range is 2×10^3 counts per second and the chart speed is $5 \text{ mm}/^\circ 2\theta$.

The samples were scanned for a 2θ range from 0 to 90° . All the samples had maxima around 32° corresponding to a d-value of around 2.79\AA , which clearly identifies with the chloroapatite (Calcium Halophosphate) structure. A typical pattern is given in Fig. 3A.

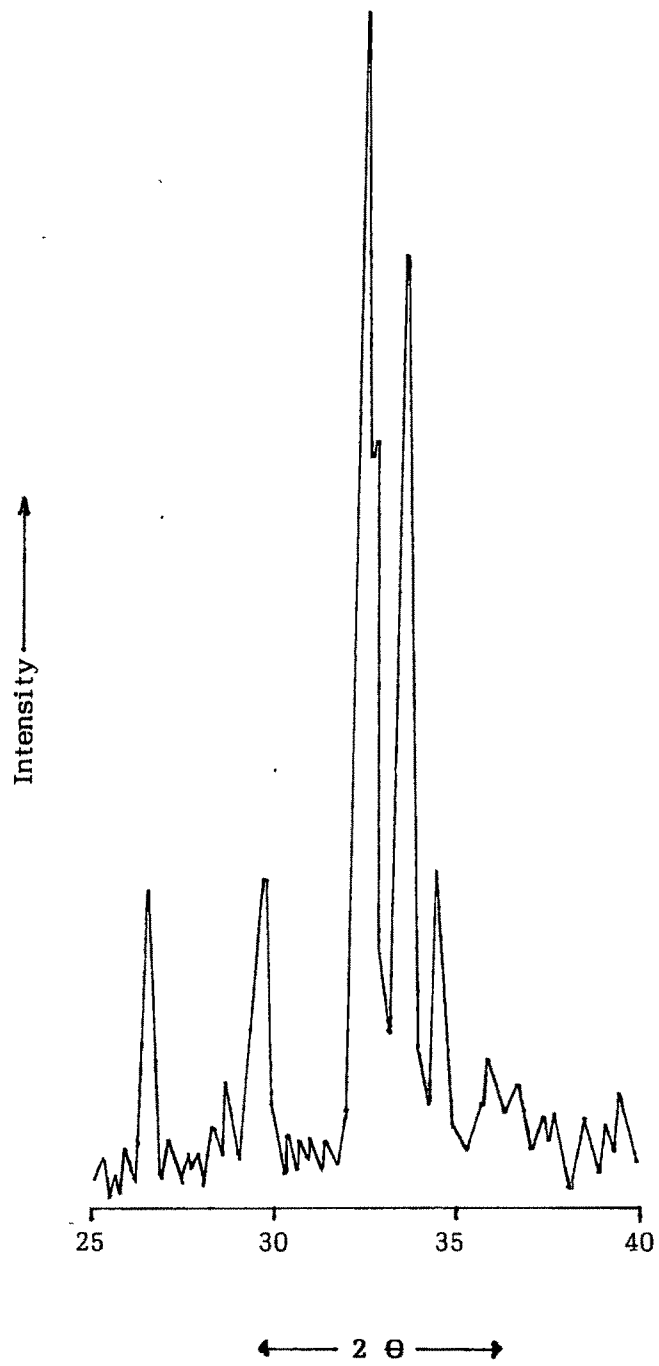


Fig. 3A : XRD Pattern of a typical sample (Calcium halophosphate).

The figure shows XRD pattern within a 2θ range of 25° to 40° , as the relevant peaks are in this section only. All the samples show identical XRD patterns. The samples have a blend of chlorofluoroapatite and agree well with the reported values [1] and ASTM card data. It is common knowledge that the phosphors used are chlorofluoro apatite with a suitable chlorine/fluorine ratio as this is required to have proper colour rendition Index (CRI) [2]. The dopants i.e. antimony and manganese also play a major role in deciding the colour. They are in very small quantities and replace the Calcium atoms in the lattice.

The crystal structure of apatites are well documented [3]. They crystallize in the hexagonal system. The space group symmetry of fluoroapatites is $P6_3/m$, while chloroapatites have a lower space group symmetry given by $P6_3$. The lower space group symmetry is due to the lack of glide mirror plane perpendicular to the screw axis in the C direction. In fact, the position of the halide ion is responsible for this.

There can be two different cationic (Ca^{+2}) sites in such systems.

- (i) At the centre of a slightly distorted tricapped trigonal prism constituted by nine oxygen atoms giving point group symmetry C_3 (site M_1).
- (ii) Six oxygen atoms of the PO_4^{3-} network with one halide ion giving point group symmetry C_{1h} (site M_{11}).

The halide ions are present on the screw axis, which is perpendicular to the plane of the triangles. The position of these ions, whose occurrence is decided by the shape, size and charge of the ion, determines the symmetry plane present [4]. The fluorine ions, due to their small size are on the plane of the triangles formed by the divalent cations, while the chloride ions owing to their bigger sizes are placed slightly off the planes of triangles

The chloroapatite crystals have a slightly different i.e. monoclinic structure and there is a change in phase to hexagonal structure at 200° C [5]. This process being reversible, it has no significance to the present work

The XRD pattern confirmed the bulk structure. However, the dopants being in very small quantity, their presence can be detected authentically by other means. One such technique is the fluorescence measurement, which is much simple and easier compared to other techniques involving chemical microanalysis or atomic absorption. The technique is based on the fact that different dopants and codopants emit different wavelengths under a given excitation wavelength in a particular host lattice. There is only a slight change in the position of emission peaks with change in concentration and temperature [6].

As in the case of XRD, which gave similar pattern for all the samples, the emission spectra of the samples for an excitation of 254 nm gave identical peaks for all the samples. One peak was around 474 nm while the other around 557 nm, which agrees well with the reported peaks for Antimony and Manganese respectively [7]. Details are given later. A typical emission spectra is given in **Fig. 3B**.

Quantum Efficiency:

The function of the phosphor is to convert the incident ultraviolet radiation into visible light. The efficacy of this conversion is the most important criteria for selection of a phosphor.

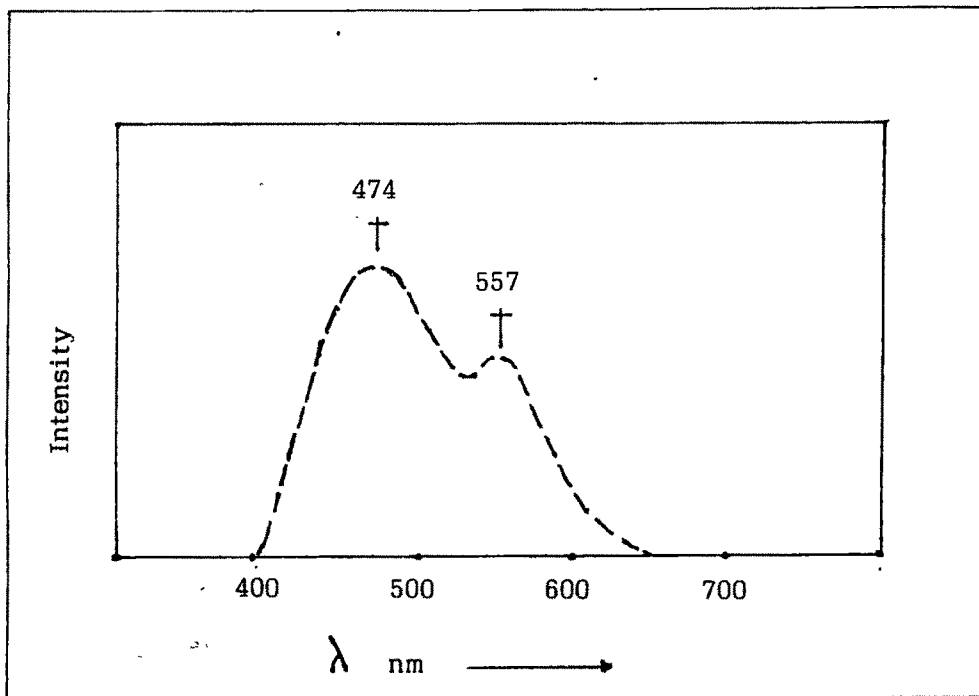


Fig.3B : Emission spectra of a halophosphate sample with Antimony and Manganese as activators. The peaks correspond to emission by Antimony (474 nm) & Manganese (557 nm).

Quantum efficiency is defined as the ratio of number of photons emitted to that absorbed by the phosphor (Q). The QE of samples were measured by direct optical method. A silicon photo diode having flat spectral response was used as detector. QE was calculated from the measured photogenerated current. Description of the instrument is given in Chapter 2.

The number of UV photons striking the phosphor surface for excitation is determined by measuring the number of reflected photons per second from a standard Magnesium Oxide (MgO) powder of known reflectivity ρ (=0.97) [8] for UV radiation. The MgO powder is loaded in an aluminium plaque. The reflected UV photons per second from MgO falling on the silicon photo diode generates a photocurrent, proportional to the number of UV photons striking its surface. This current C_1 is given by

$$C_1 = k \rho Y I_e \quad \text{----- (a)}$$

where k is a constant representing the geometry of the apparatus, Y is the number of UV photons per second striking the MgO surface and I_e is the photocurrent produced in the photodiode by a single UV photon striking its surface per second, expressed in Ampere/photon/second.

The aluminium plaque is now loaded with the phosphor. The UV photons striking the phosphor gets partly absorbed and partly reflected. Thus the photocurrent C_2 generated in the photodiode is due to the combined effect of visible fluorescent emission (in number of photons per second) spread over a range of wavelengths and the reflected UV (in number of photons per second). If C_3 is the photocurrent due to fluorescent emission and C_4 due to the reflected UV, then

$$C_2 = C_3 + C_4 \quad \text{----- (b)}$$

As the quantum response of the photodiode in the visible region is flat, C_3 can be written as,

$$C_3 = KQ(1-r)YI_f \quad \text{----- (c)}$$

and

$$C_4 = KrYI_e \quad \text{----- (d)}$$

Where Q is the quantum efficiency, r is the reflectivity of the phosphor for UV and I_f is the photocurrent generated in the photodiode by a single fluorescent photon striking its surface per second, expressed in Amperes per photon per second. Substituting for Y in terms of C_1 from equation (a) in equation (b),

$$\frac{C_2}{C_1} = \frac{[(1-r)QT_f]}{I_e} + \frac{r}{\rho} \quad \text{----- (e)}$$

From equation (e), the final expression for Q can be given as,

$$Q = \frac{C_3}{C_1} \frac{I_e}{I_f} \frac{\rho}{1-r} \quad \text{----- (f)}$$

Where $r = \rho(C_4 / C_1)$ from equation (a) and (d).

This is a brief mathematical treatment of the equation for Quantum efficiency. A detailed description is given in Chapter 2.

The value of Q is determined from equation (f) by substituting all the known values in which C_1 and C_3 are actually measured and I_e and I_f are deduced from the characteristic curve of the silicon photodiode (**Fig. 3C**). To measure C_1 , the aluminium plaque is loaded with MgO and placed in the apparatus and the UV radiation is focused onto a small area using a quartz lens. The reflected UV rays from MgO produce the photocurrent C_1 in the photodiode, which is measured by the electrometer amplifier. The plaque is now emptied and filled with the phosphor for measuring its quantum efficiency. As before, the current C_2 is now measured. The Pyrex glass filter is then placed in front of

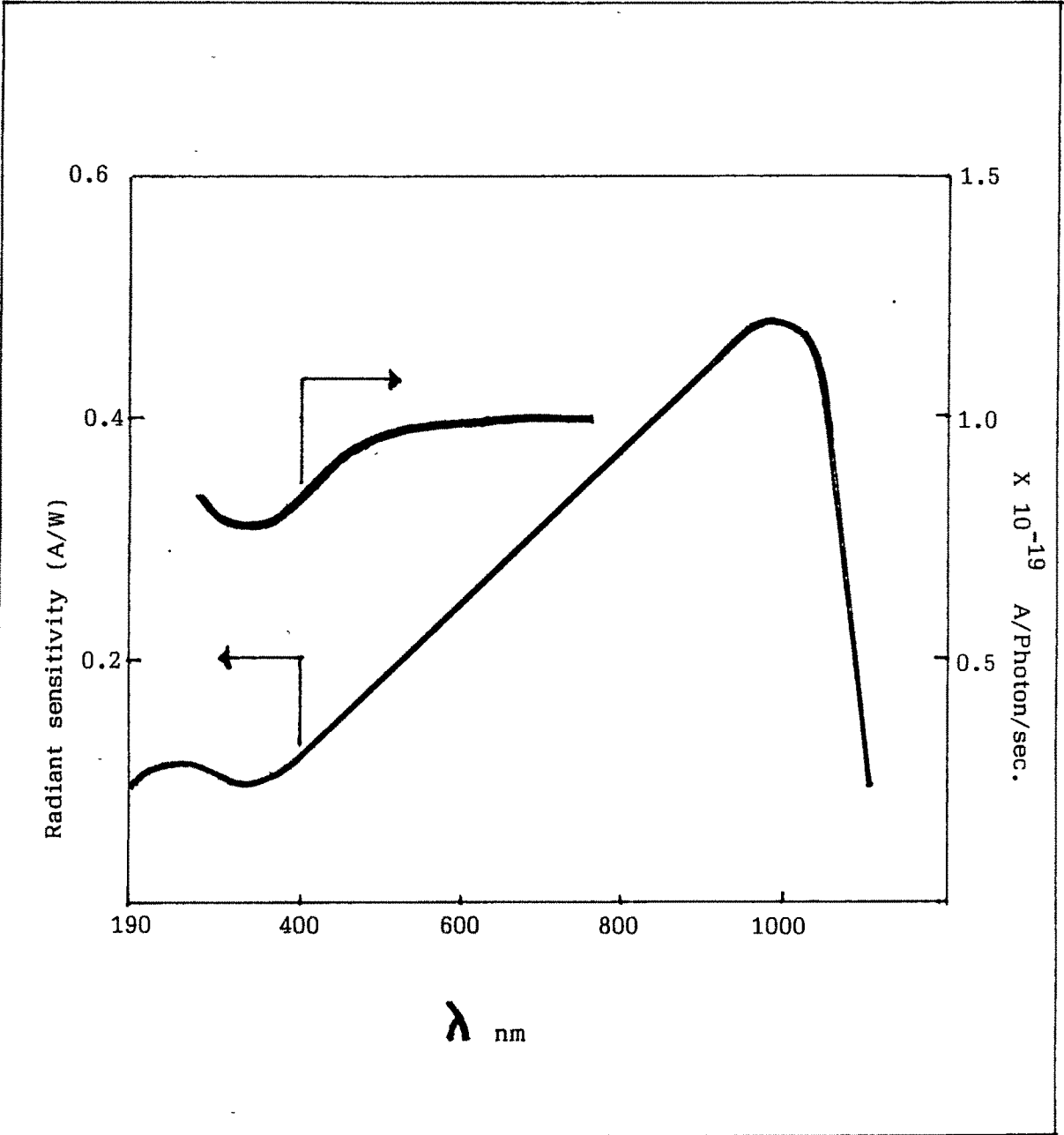


Fig. 3C : Spectral response characteristics of photodiode, Type No. S 1337-1010 BQ. (Reproduced with courtesy - Hamamatsu.)

the photodiode to cut off the reflected UV rays from the phosphor and the current due to the remaining fluorescent radiation C_3 alone is also measured.

From these measurements, we get,

$$C_4 = C_2 - C_3.$$

Precisely, this C_3 is not the current component in C_2 due to fluorescence alone. The measured current is equal to C_3^1 , which is an alternated value of C_3 due to the transmission coefficient τ_f of the Pyrex filter. The real current C_3 is equal to C_3^1 / τ_f . The transmission coefficient τ_f was measured on a Shimadzu spectrophotometer and its value found to be $0.92 \pm 1\%$ for the visible region of emission. When all unknowns in equation (f) are thus determined, quantum efficiency of any phosphor can be calculated.

Going back to the spectral characteristics, the quantum response of the silicon photodiode type no. S1337-1010 BQ is not flat in the UV region. However, this does not cause any significant error in the measurement, since the wavelength of the exciting UV photon is known before hand and the current I_e which it generates in the photodiode can be precisely determined from the characteristic curve and substituted in equation (f). The flatness of the quantum response of the silicon photo diode results from the creation of the same number of electron hole pairs in the active volume of the diode (which contributes to photogenerated current) by a photon of energy higher than the band gap of silicon i.e. 1.1 eV ($\lambda = 1100$ nm) up to an energy of 5 to 6 eV (UV radiation), striking its photosensitive surface. The value should remain unity and the photogenerated current due to it should be $2 \times 1.6 \times 10^{19}$ A, where 1.6×10^{-19} is the charge of an electron in coulomb. However due to physical changes occurring during diode processing and the reflectivity variations of the diode surface with wavelength, the actual photogenerated current from the diode characteristic curve appears to be much less than 3.2×10^{19} A. But it remains reasonably constant for all photons in the visible region, which can be approximated to a flat quantum response.

The measured value of Q needs to be corrected for the reflectivity of the phosphor for its own emission, to obtain the true or intrinsic quantum efficiency Q_i given by,

$$Q_i = 2Q / 1 + R_\infty$$

where R_∞ is the reflection coefficient of an infinitely thick layer of phosphor for its own emission. The value of R_∞ is close to unity and hence the value of Q and Q_i are almost the same

The Quantum efficiencies of the samples were measured on such an apparatus at the Rare Earth Development Section of B.A.R.C, Bombay. The measured values of currents are given in **Table 3.1**.

Table 3.1 :

Sample	Photo-currents $\times 10^{-11}$ A					Quant. Eff Q. %
	C_1	C_2	C_3^1	C_3	C_4	
Ref (MgO)	24					
P-1	24	33	23	25	8.0	83.02
P-2	24	34	25	27.2	6.8	86.09
P-3	24	33	25	27.28	5.8	82.81
P-4	24	35	26	28.6	6.4	89.45
P-5	24	34	26	28.26	6.4	85.86
P-6	24	34	24	26.1	7.9	84.43

Here,

C_1 is the photocurrent, when MgO is loaded in the plaque,

C_2 is the photocurrent without keeping pyrex filter when the phosphor is loaded in

the plaque,
 C_3 is the photocurrent after keeping pyrex filter,

$C_3 = C_3^1 / \tau_f$, where τ_f is the transmission coefficient of the pyrex glass filter = 0.92,

$C_4 = C_2 - C_3$, which gives the reflected component of UV by the phosphor, and

$Q = (C_3 / C_1) \times (I_e / I_f) \times (\rho / 1-r)$ is the quantum efficiency expressed in percentage in the table.

From the table, it is clear that sample P-4 has the maximum quantum efficiency followed by P-2 and P-5. Samples P-6, P-1 and P-3 take the last three positions in descending order.

The component C_4 i.e. $C_2 - C_3$ also becomes significant as it gives a measure of the UV radiation reflected. The samples P-1 and P-6 having comparatively lower Quantum efficiencies have a higher value of C_4 i.e. they reflect more amount of UV radiation incident on them. On the other hand samples P-2, P-4 and P-5 have comparatively lower values of C_4 indicating less reflection of incident UV radiation. Sample P-3 has in contrast a lower value of C_4 inspite of its lowest Quantum Efficiency. The lower quantum efficiency can be also attributed to non-radiative processes within the phosphor material.

The values of Quantum efficiency given in the table are in agreement with the reported values. Quantum efficiencies of Calcium Halophosphates doped with Antimony and Manganese range from 52% to 96% [9-12]. The phosphors used commercially have high quantum efficiencies as they have to be viable, e.g. halophosphates and blends of halophosphates used by Philips have quantum efficiencies ranging from 84% to 90%.

The quantum efficiency is dependent on the effective absorption of the UV radiation of 253.7 nm, which in turn depends on the phosphor quality viz. its crystallinity, the grain size distribution (ball milling in excess can have a negative effect on quantum efficiency), presence of impurities (leading to transfer of energy to killer centres, which utilize the energy for non-radiative transitions) and other factors [13].

Excitation Spectra:

The excitation spectra was recorded on a Hitachi make fluorescence spectrophotometer (Model No F-4010), in which the excitation beam is automatically corrected for intensity variations of the source with wavelength. The detector used is the Hamamatsu make, photomultiplier (PMT) (type no R955 of multi-alkali photocathode) which has a flat spectral response over the entire range of wavelength of measurement from 200 nm to 900 nm.

As stated earlier, calcium halophosphates doped with Antimony and Manganese are characterised by emission peaks of 474 nm and 557 nm for the former and later respectively. Hence the excitation spectra was scanned for these two values of monitoring emission lines. The peak excitation wavelengths and their respective intensities are given in Table 3.2.

Table 3.2 :

Sample	Monitoring line (nm)	Peak (nm)	Intensity Rel. Units
P-1	474	280	468.3
	559	280	320.5
P-2	473	277	1436
	554	277	1078
P-3	476	276	379.9
	857	278	261.8
P-4	472	276	1831
	557	278	1213
P-5	478	272	1144
	557	274	838.9
P-6	476	274	987.1
	559	278	781.1

For taking the excitation spectra, equal quantities of phosphor were taken for each sample and the emission spectra of each of the sample was recorded for an excitation wavelength of 254 nm. Each sample gave two peaks. These peaks were taken as monitoring line for the excitation spectra. Hence different monitoring wavelengths for different samples. The excitation spectra are given in **Figs. 3D - I to 3D - VI**.

The excitation intensity is maximum for P-4 followed by P-2, P-5, P-6, P-1 and P-3 in that order. This is the same order in which quantum efficiency of the samples are placed.

It can be seen from the curves and tables that the peak excitation is not exactly at 254 nm but between 270 nm to 280 nm. Peak excitation values lower than these i.e. about 254 nm are desirable for maximum absorption of the 254 nm radiation emitted by the low pressure mercury discharge. For the 557 nm monitoring line, there are additional peaks around 350 nm and 408 nm having much lower intensity.

The incident UV energy is absorbed by the crystal lattice of the halophosphate. A part of this energy is consumed as lattice vibration energy while a substantial amount is transferred to antimony atoms. The antimony gets excited by undergoing a transition from 1s ground state to excited 1p and 3 p states. The excited antimony atoms transfer fraction of the energy of excitation to the manganese ions, which undergo 3d → 3d transition.

Emission Spectra :

The emission spectra was also recorded on the same instrument on which the excitation spectra was recorded, which has been described in Chapter 2.

The emission spectra were recorded for an excitation wavelength of 254 nm.

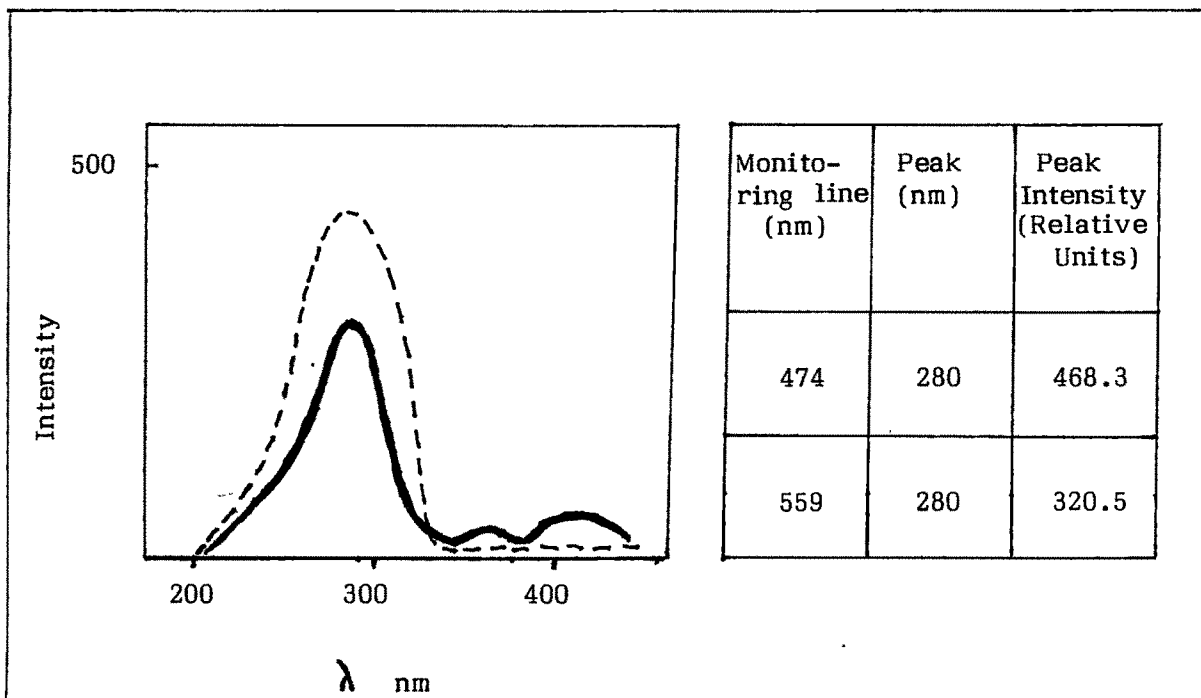


Fig. 3D-I : Excitation spectra for sample P-1.

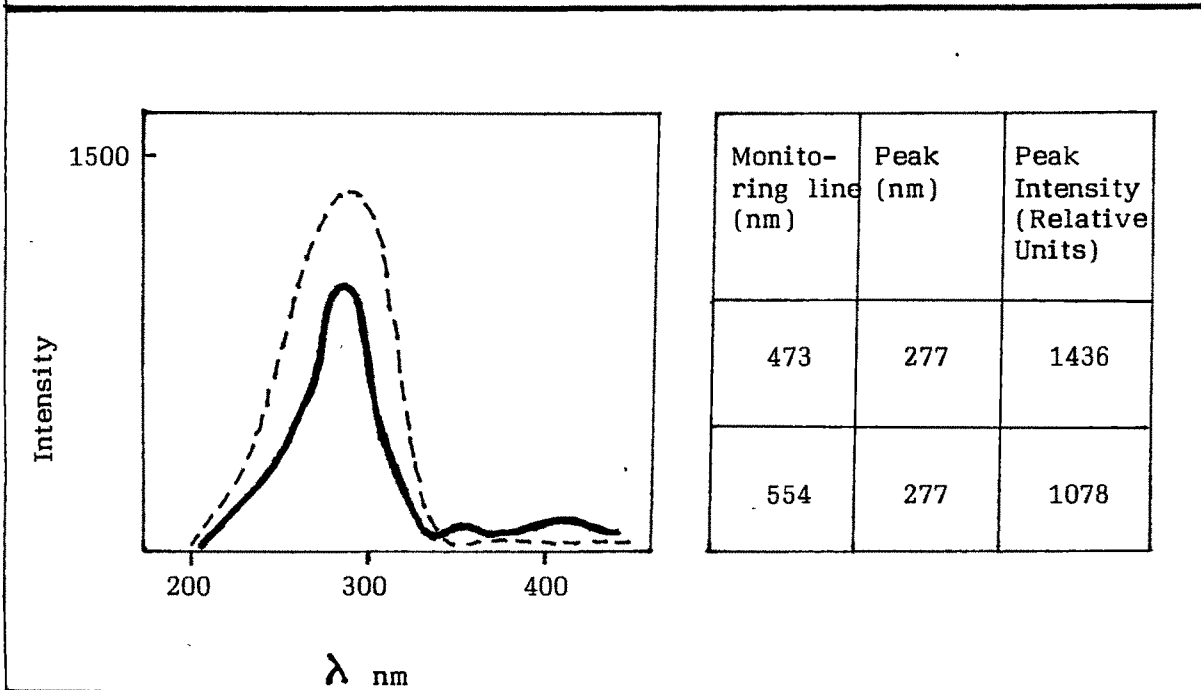
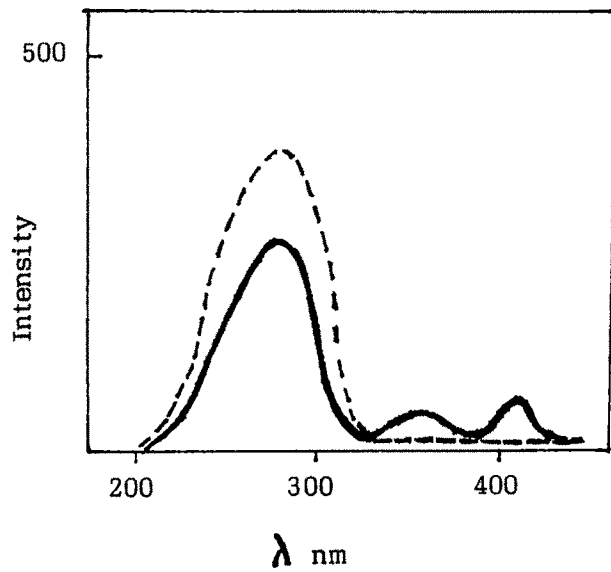
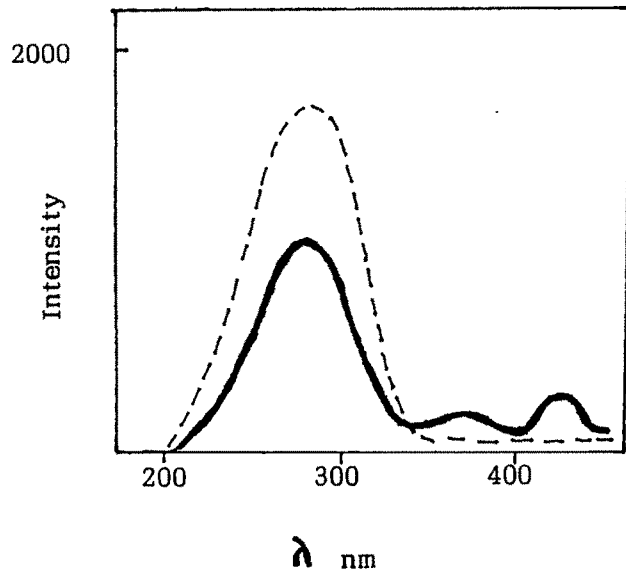


Fig. 3D-II : Excitation spectra for sample P-2.



Monitoring line (nm)	Peak (nm)	Peak Intensity (Relative Units)
476	276	380
557	278	262

Fig. 3D-III : Excitation spectra for sample P-3.



Monitoring line (nm)	Peak (nm)	Peak Intensity (Relative Units)
472	276	1831
557	278	1213

Fig. 3D-IV : Excitation spectra for sample P-4.

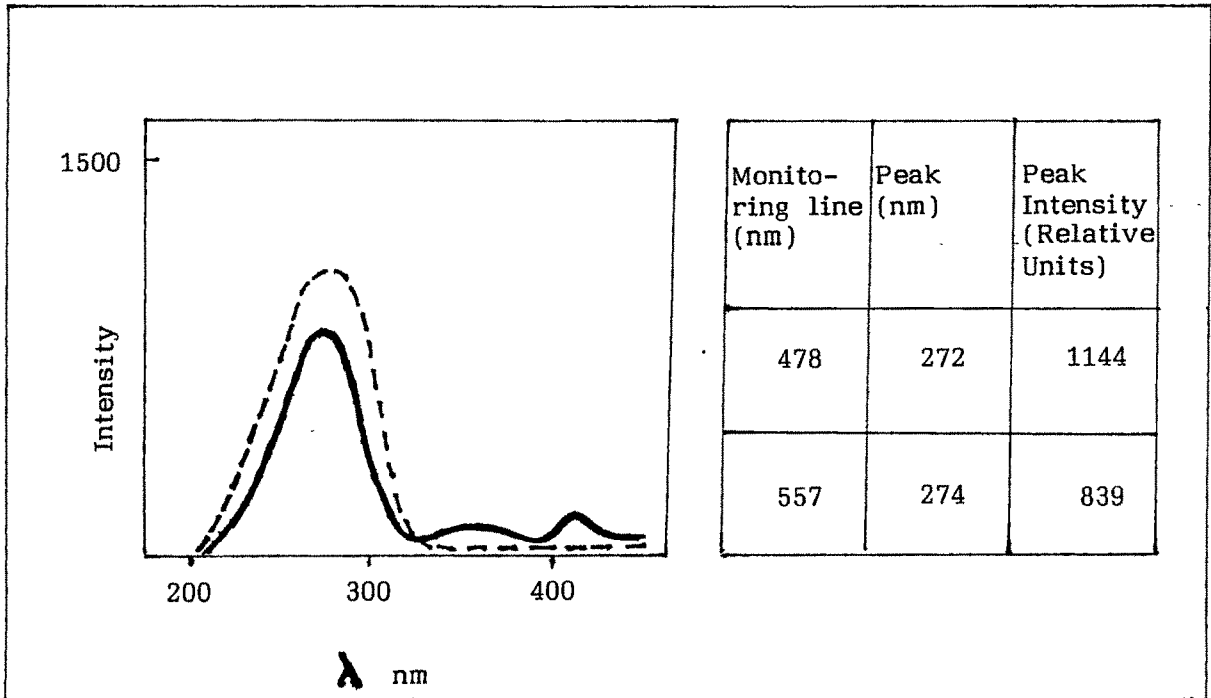


Fig. 3D-V : Excitation spectra for sample P-5.

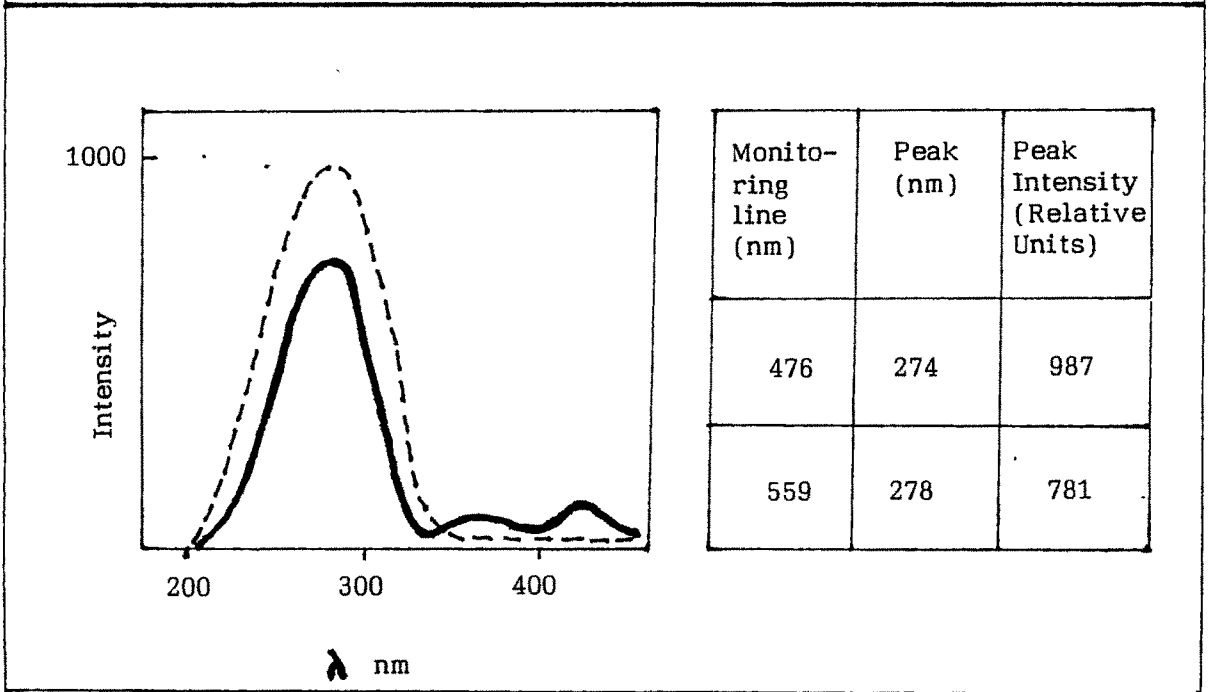


Fig. 3D-VI : Excitation spectra for sample P-6.

The maximum emission intensity was recorded for sample P-4 followed by P-2, P-5, P-6, P-1 and P-3 in that order. Here again, the order observed in case of quantum efficiency and intensity of excitation has been maintained. The emission spectra are given in **Figs. 3E - I to 3E - VI**.

It has been mentioned earlier that part of the energy absorbed by the antimony atoms is transferred to the manganese while another part of the energy is emitted by the antimony transition from excited 1p and 3 p singlet to the lowest-lying triplet p state. This emission is in the blue region around 474 nm. The energy transferred to manganese ions manifests itself into emission around 557 nm by virtue of 3d --> 3d transition.

In these calcium halophosphates activated by antimony and manganese, a small portion of calcium atoms are replaced by trivalent antimony ions and bivalent manganese ions. Some of the fluorine atoms are replaced by chlorine atoms. The location of the antimony emission line is reported to be independent of composition, whereas that of manganese band is governed by the ratio of chlorine to fluorine to certain extent. Greater the ratio, the wavelength shifts towards the longer side. The position of this band also changes on account of the quantity of manganese. Both antimony and manganese ions replace those Ca^{2+} ions which are in the vicinity of halogen ions. When Sb^{3+} ion is incorporated, the adjacent halogen ion is replaced by an O^{2-} ion to maintain electrical neutrality. The antimony ions are not therefore, in direct contact with the halogen ions and the substitution of chlorine for fluorine will have little effect on the excitation of antimony. On the other hand, bivalent manganese ions are in the vicinity of halogen ions and the emissivity of the manganese is definitely affected by the substitution of fluorine by chlorine.

Literature available on energy transfer mechanism in solids [14,15] suggest a few ways of energy transfer between sensitizer and activator. These can be categorised as under .

- (i) Energy transfer by movement of charge carriers

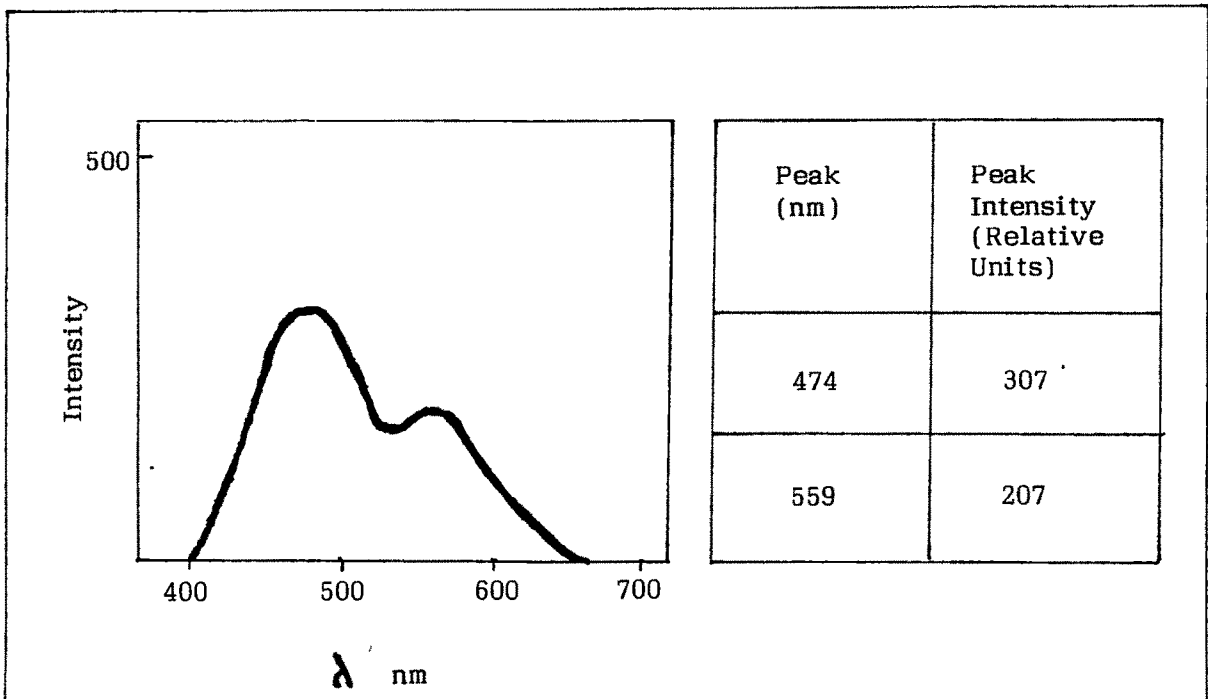


Fig. 3E-I : Emission spectra of sample P-1. Excitation - 254 nm.

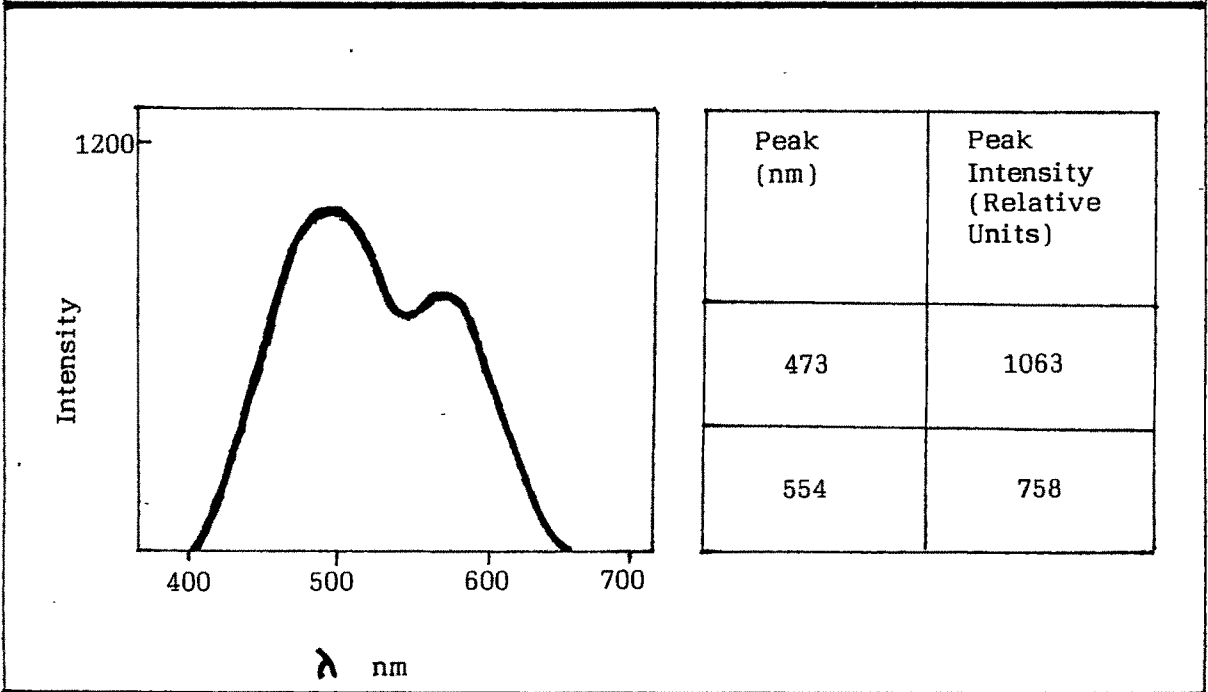
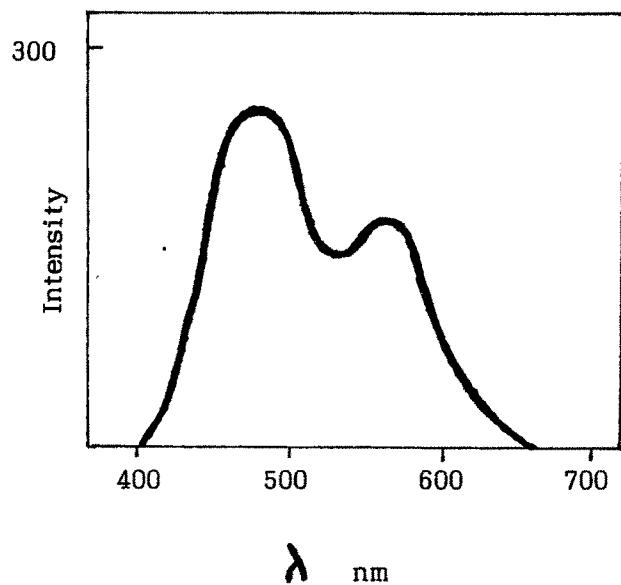
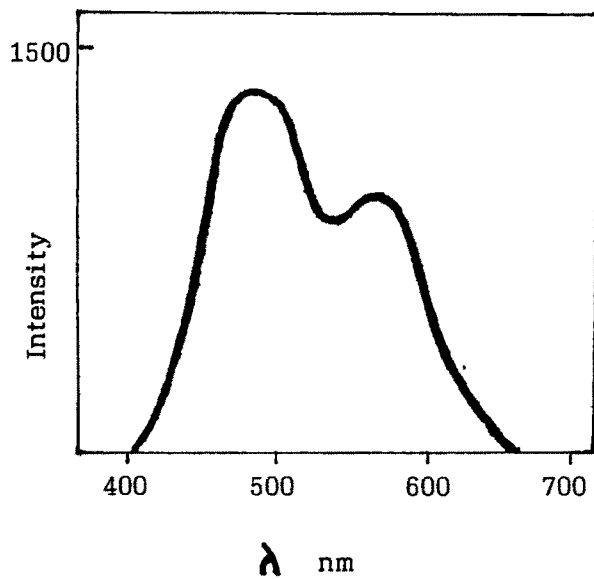


Fig. 3E-II : Emission spectra of sample P-2. Excitation - 254 nm.



Peak (nm)	Peak Intensity (Relative Units)
476	253
557	175

Fig. 3E-III : Emission spectra of sample P-3. Excitation - 254 nm.



Peak (nm)	Peak Intensity (Relative Units)
472	1314
557	855

Fig. 3E-IV : Emission spectra of sample P-4. Excitation - 254 nm.

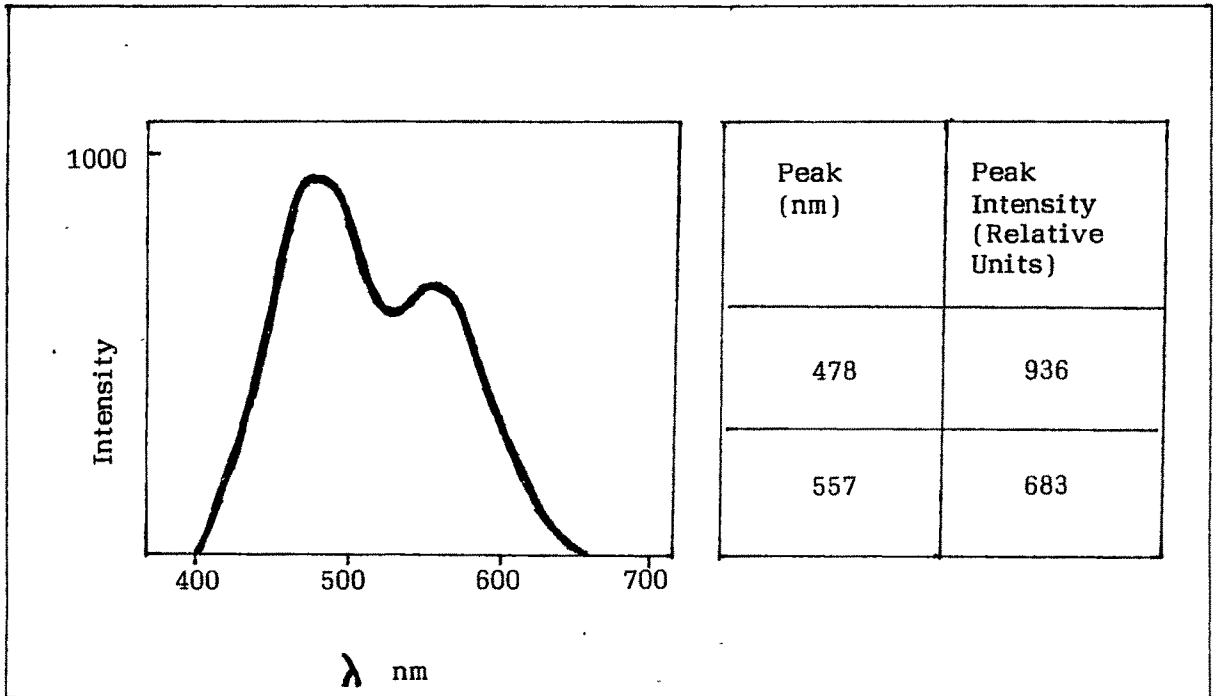


Fig. 3E-V : Emission spectra of sample P-5. Excitation - 254 nm.

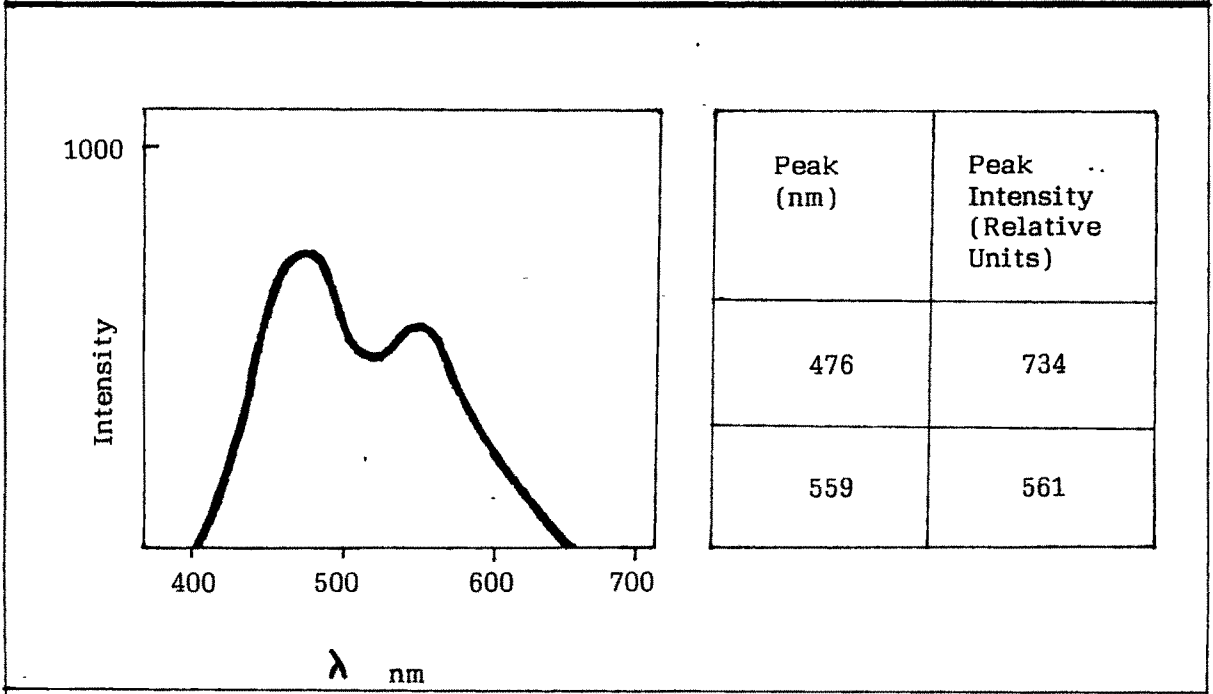


Fig. 3E-VI : Emission spectra of sample P-6. Excitation - 254 nm.

- (ii) Radiative transfer by emission by the sensitiser and absorption by activator.
- (iii) Non-radiative transfer associated with resonance between sensitiser and activator

Neglecting energy transfer by the movement of charges, the other two modes become more relevant in case of solids. The probability of radiative transfer depends on how efficiently the activator fluorescence is excited by the sensitiser emission. It requires a significant overlap of the emission region of the sensitiser and the absorption region of activator and an appreciable intensity of absorption of activator. In view of the later requirement, radiative transfer does not often occur in inorganic systems. The overlap region in this case being relatively small, this might not be the dominant mode of energy transfer. Besides the intensity of absorption cannot be known with a degree of authenticity to put conclusive remarks

Thus one is left with the other mode of non-radiative energy transfer in which two types assume particular significance in solids. One by electric multipole interactions and another by exchange interaction. Transfer by exchange is restricted to nearest neighbours. Transfer by multipole interactions can be of importance even over distances of 20-30 Å. The manganese ions being surrounded by halogen atoms, the exchange mechanism does not seem to be the likely mode. Hence transfer by multipole interaction seems to be the dominant mode of energy transfer.

Qualitative characteristics of Lamps :

There are two main indicators of the quality of lamp (i) Intensity of light given in terms of Lumen and (ii) Colour rendering property given by colour coordinates or CRI. The properties mentioned above are taken under standard electrical conditions, given as under :

Wattage	40 W
Input voltage	220 V

Voltage variation	$220 \pm 0.5V$
Voltage across the lamp	$103 \pm 10 V$
Starting voltage	$108 \pm 1 V$ at $25^{\circ} C$
Frequency variation	$50 \pm 0.2 Hz.$

The light output in lumens is recorded after burning the lamp for 100 hours

Light Intensity (Lumen Output) :

The light intensity is measured in terms of lumen. The device used for measurement is a spherical chamber called Integrator. The light intensity at a particular point of the integrator is measured in terms of photocurrent using a silicon photo diode having a flat quantum response in visible region. The photocurrent is integrated over the entire inner surface of the integrator and the reading of the light output can be noted directly.

Table 3.3 shows the lumen output for each of the lamps and their average in each category. It has been mentioned earlier that readings of five lamps in each category, selected on a random basis are available.

Table 3.3 :

Sample	Lumen Output Lumens	Average Lumens
P-1	2371	2399
	2392	
	2429	
	2456	
	2348	
P-2	2487	2503
	2505	
	2499	
	2526	
	2499	

P-3	2384	2391
	2337	
	2368	
	2420	
	2446	
P-4	2511	2520
	2501	
	2537	
	2520	
	2532	
P-5	2463	2487
	2509	
	2478	
	2488	
	2496	
P-6	2440	2442
	2389	
	2465	
	2482	
	2435	

The table shows that the maximum average lumen output is for the sample P-4 followed by P-2, P-5, P-6, P-1 and P-3 in that order. This order is the same as that of quantum efficiency of the samples. Although this can be expected, the unusual thing about these results is the extent of variation in lumen output for various lamps made from the same phosphor. This aspect calls for the consideration of factors related to the manufacturing process as all other factors are identical for the samples.

Theoretically, the maximum output of 76 lumen/watt i.e. about 3000 lumens for a 40 watt lamp can be obtained. It can be seen however that the output of the lamps are much below the theoretical maximum. The value prescribed by ISI is 2450 lumens. The electrical and geometrical parameters of lamps also play a significant role.

Colour Points :

Talking about quality of a lamp, apart from a good light output, its colour rendition characteristic is also important. The ultimate in this regard is a lamp that faithfully replicates the white light. Hence the measure of good colour rendition is the proximity to the so called 'white' point in the chromaticity diagram.

The colour rendition of a luminous object depends upon its spectral characteristics, which can be described in the form of coordinates of chromaticity diagram also called colour points. The measurement of the colour points was done using a device of 'Minolta' make, specially meant for the purpose. It gives direct reading of the 'x' and 'y' coordinates. The working of such an instrument is given in Chapter 2

The colour coordinates of the five lamps in each category are given in **Table 3.4**.

Table 3.4 :

Sample	X - coordinate		Y - coordinate	
	Individual	Average	Individual	Average
P-1	0.315	0.3154	0.341	0.3404
	0.315			
	0.316			
	0.317			
	0.314			
P-2	0.318	0.3168	0.346	0.3452
	0.318			
	0.315			
	0.318			
	0.315			
P-3	0.315	0.3156	0.341	0.3406
	0.317			
	0.315			
	0.314			
	0.317			

P-4	0.314	0.3146	0.345	0.3466
	0.314		0.345	
	0.317		0.349	
	0.314		0.345	
	0.314		0.349	
P-5	0.315	0.315	0.346	0.3484
	0.318		0.349	
	0.316		0.349	
	0.318		0.349	
	0.318		0.349	
P-6	0.319	0.3162	0.345	0.345
	0.316		0.344	
	0.314		0.345	
	0.314		0.345	
	0.318		0.346	

These colour coordinates obviously depend upon the emission characteristics of the phosphor to a large extent. The visible lines of mercury which are mainly in the violet and blue region also play a small part as some of the emission from mercury is absorbed by the phosphor. The fluorescent lamps are categorised into several types like cool daylight, white, warm white, etc. depending upon the position of its colour point with respect to the black body locus in the chromaticity diagram. Few of such points are shown in Fig. 3F.

The colour coordinates in Table 3.4 can be matched with the prescribed values for the different categories of lamps mentioned above. Comparing with specifications of Philips, the colour point comes nearest to the 'cool daylight' variety, for which the colour coordinates are $x = 0.309$ and $y = 0.327$ corresponding to a colour temperature of 6750°K .

In general, the halophosphate category of phosphors are assigned to a specific locus point in the chromaticity diagram (Fig. 3F) [16]. In view of the varied spectral

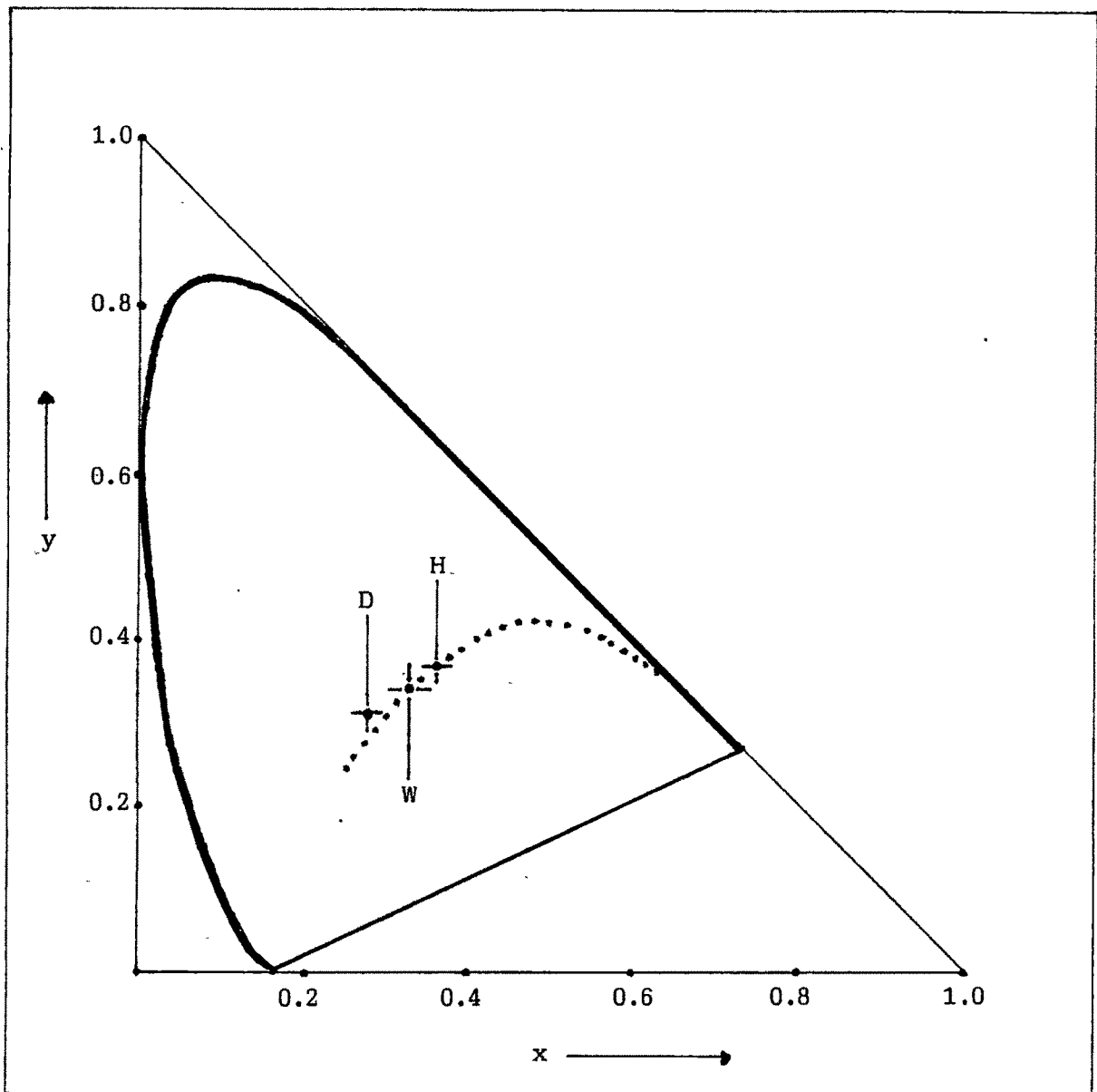


Fig. 3F : Chromaticity diagram with black-body locus showing chromaticities of the full radiator. (Dotted line)

D - Colour point of 'Daylight' variety of fluorescent lamp.

H - Colour point corresponding to Halophosphate phosphors.

W - Colour point of 'White point'.

characteristics of different halophosphates, it seems that the colour points would be scattered over a particular region.

Grain size distribution:

Grain size is one of the significant parameters of the phosphor material. It is generally believed that the grain size should be as small as possible. However, there can be an optimum range. The grain size plays an important part in the absorption of incident radiation. The grain size distribution of the samples is given in Table 3.5.

Table 3.5 :

Particle size (micron)	Volume (%)					
	P-5	P-2	P-3	P-4	P-1	P-6
1.32	1.85	1.38	1.17	1.11	0.66	1.39
1.60	1.52	1.99	1.65	1.49	1.01	1.60
1.95	1.19	2.15	1.78	1.45	1.14	1.33
2.38	0.80	1.97	1.72	1.04	1.04	0.96
2.90	0.87	1.72	1.80	0.56	0.81	1.01
3.53	1.87	1.77	2.33	0.54	0.67	1.99
4.30	3.99	2.47	3.52	1.47	0.99	4.07
5.24	7.10	4.01	5.43	3.47	2.01	7.23
6.39	11.09	6.36	7.88	6.36	3.87	11.01
7.78	14.59	9.23	10.35	9.95	6.49	14.33
9.48	16.44	12.32	12.32	14.24	9.83	16.05
11.55	15.14	14.72	13.11	17.87	13.41	14.93
14.08	11.47	14.69	12.27	17.22	15.42	11.52
17.15	7.11	11.88	10.04	12.46	14.98	7.22
20.50	3.43	7.62	7.10	6.89	12.22	3.48
25.46	1.12	3.82	4.27	2.86	8.36	1.11
31.01	00.08	00.31	02.07	00.60	04.60	00.06
37.79		00.15	00.71		01.88	
46.03			00.06		00.42	
Percentage of particles between 8 to 17 microns	65	70	58	72	60	64

The lamp industry in India has been found to be using phosphors having grain size between 7 to 17 microns. However in all the cases, the grain size is almost entirely below 25 microns, as the amount of particles beyond that size is insignificant. For the better performing phosphors, this is below 1%. It is common knowledge in lamp processing that too much ball milling, required for smaller grain size brings down the efficiency. On the other hand, bigger grain size leaves interstices between the grains, through which the UV radiation passes into the glass surface, leading to a loss of excitation energy. Hence an optimum size has to be considered. An optimum range of grain size has been proposed here between 8 to 17 microns approximately. This is because the average particle size is between 12 to 13 microns and maximum number of particles are covered by the proposed range (i.e. 12.5 ± 4.5 microns). It can be seen from the table that the maximum percentage of grains in this range has been found for sample P-4, followed by P-2, P-5, P-6, P-1 and P-3.

As stated earlier, the maximum lamp output is expected from low grain size phosphor. The particle size reported is around 5 microns [17]. Using low grain size would also reduce the amount of phosphor used and save upon the cost of production. However getting such small uniform grain size is a bit difficult as it needs prolonged ball milling, which can effect the structure of material. Smaller grain size can be achieved by wet chemical process.

Correlation :

It is obvious that the purpose of this work is to correlate the parameters discussed above, to draw a model to identify a better phosphor. Here again, the discussion would be centred around the two deciding factors about the quality of the lamp namely, light output and colour rendition.

The light output of a fluorescent lamp is a direct function of the efficiency with which the UV radiation is converted into visible, which is given by the parameter quantum efficiency. It can be seen from **Fig. 3G** that the light output increases with increase in quantum efficiency.

Although it can be inferred that the light output of lamp increases with increase in the quantum efficiency of the phosphor used, the variation has not been found to be strictly linear. It would be easier to predict the lumen output for a given efficiency of phosphor, if the trend is linear. However the linearity here can be visualised in two directions given by segments A and B. (broken lines) Although the linear variation from P-3 to P-2 suggests the segment A to a logical consequence, this trend is quite unlikely. This is because, as per the sequence given by segment A, a lamp with a phosphor of Quantum efficiency around 89.5% (P-4) would give a lumen output of 2700 lumens approximately. On the other hand, the sequence followed by segment B is more likely. According to this sequence, the lamp output corresponding to a Quantum efficiency of around 89.5% (P-4) would be 2560 lumens. This looks more practical, as per the ISI standard of 2450 lumens/40 w. Considering this sequence i.e. of segment B, the non-linearity becomes more evident. Hence it can be concluded that other factors related to the phosphor and lamp manufacturing process play a role.

Apart from the aspect of linearity mentioned above, the different ranges of variation of lumen output in case of the lamps looks interesting (**Fig. 3H**). One has to keep in mind here that the lamps have been manufactured under similar manufacturing conditions and hence the process conditions are also same for all the lamps studied. This makes the other factors all the more important. **Table 3.6**, however points out to the common trend that has been observed so far.

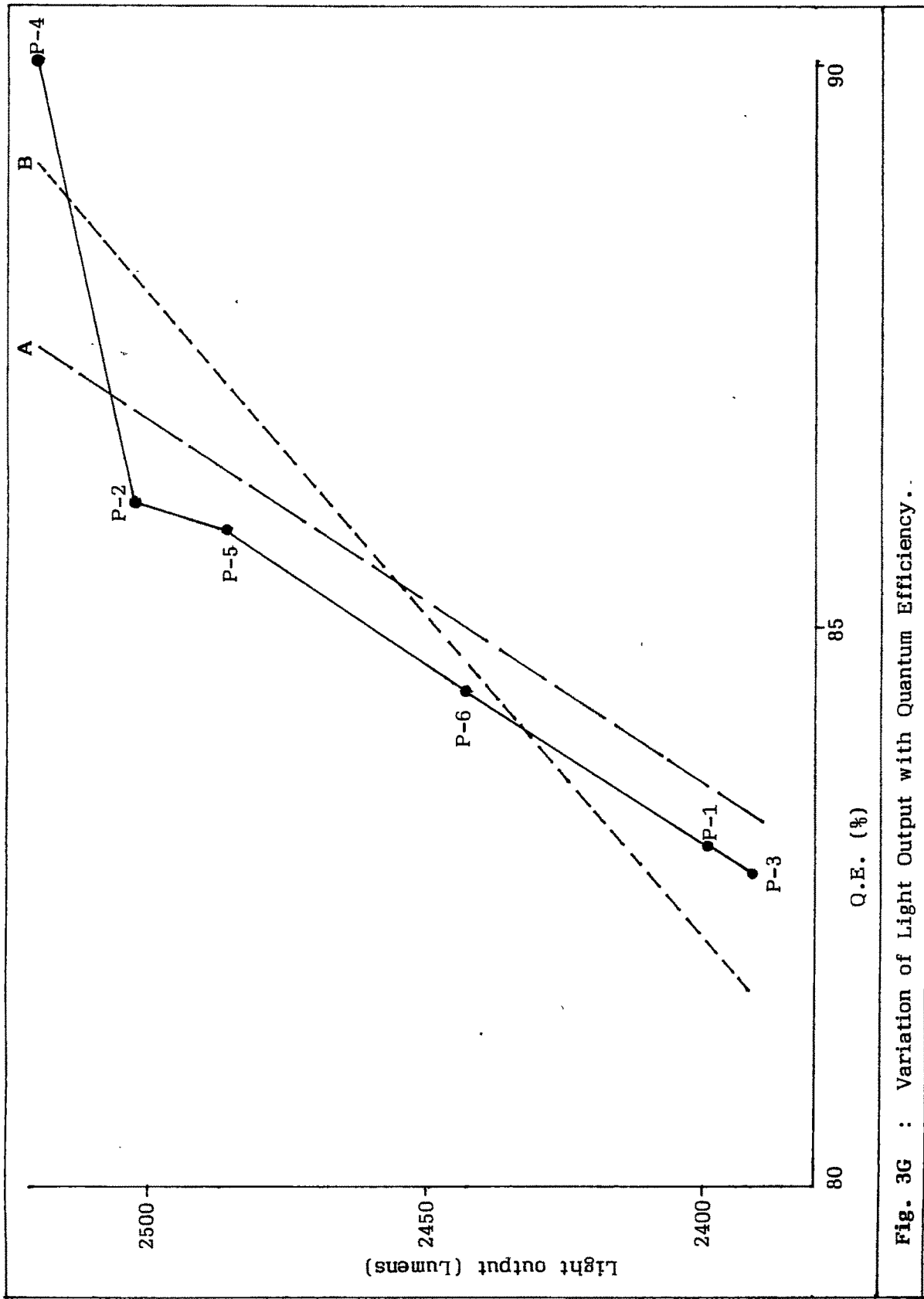


Fig. 3G : Variation of Light Output with Quantum Efficiency.

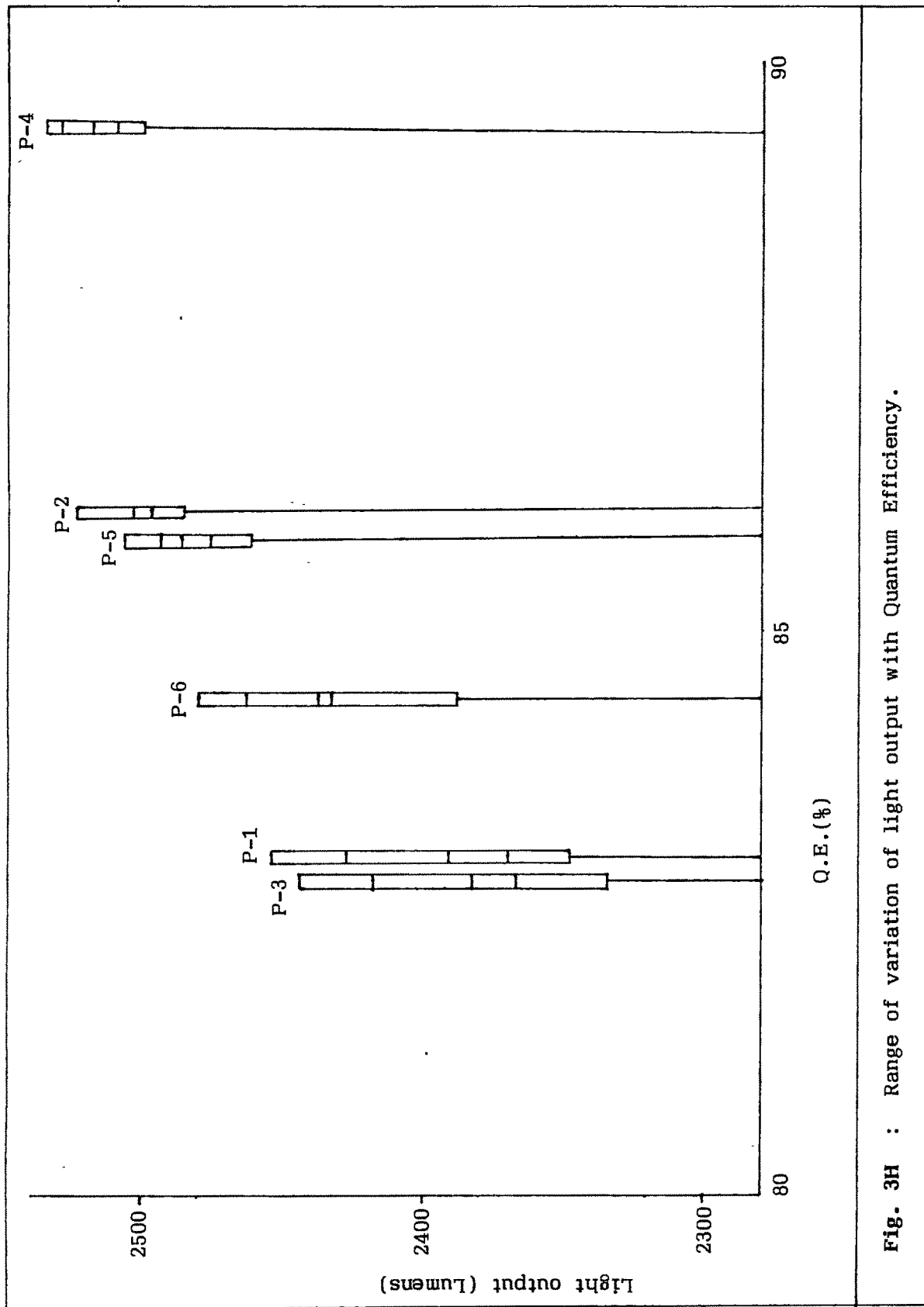


Fig. 3H : Range of variation of light output with Quantum Efficiency.

Table 3.6 :

Sample	Quantum Eff. (%)	Average Lumen output (Lumens)	Range of variation (Lumens)
P-1	83.02	2399	108
P-2	86.09	2503	39
P-3	82.81	2391	109
P-4	89.45	2520	36
P-5	85.86	2487	46
P-6	84.43	2442	93

It can be seen from the table that the range of variation is maximum for sample P-3 followed by P-1, P-6, P-5, P-2 and P-4 in the descending order. Relating this to the quantum efficiency of the samples and lumen output of the corresponding lamps, it becomes evident that better phosphor has a low range of variation. It can be again seen that the decrease in the range of variation of lumen output from P-3 to P-4 does not correspond to a linear increase in either the quantum efficiency or average lumen output. Hence one should look to the other factors. One of the parameters that is likely to be responsible for the variation is the coating thickness, as it varies from region to region inside the tube.

It has been already discussed that the two peaks of emission spectra, correspond to emission by antimony and manganese. Considering these peaks to be peak 1 and peak 2 respectively, and the process of excitation i.e. absorption by antimony and transfer of energy to manganese, it is logical to believe that more is the absorption by antimony, better would be the phosphor. Hence the intensity of excitation of peak 1, which gives the absorption by antimony should be taken into consideration. Table 3.7 shows the intensity of excitation (in arbitrary units) and the relative intensities.

Table 3.7 :

Sample	Intensity of excitation		Relative Peak 1	Intensity Peak 2
	Peak 1	Peak 2		
P-1	468.3	320.5	0.59	0.41
P-2	1436	1078	0.57	0.43
P-3	379.9	261.8	0.59	0.41
P-4	1831	1213	0.60	0.40
P-5	1144	838.9	0.58	0.42
P-6	987.1	781.1	0.56	0.44

The maximum is seen for sample P-4 for the peak 1, which has so far been the best of the samples. However the general trend has not been evident in this case, as sample P-4 is followed by P-1 and P-3, which show comparatively lower performance.

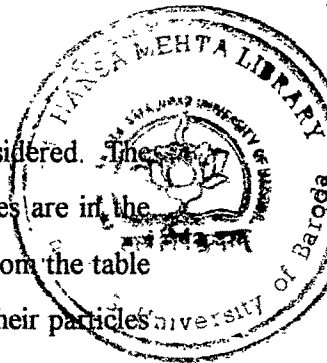
The absorption of exciting radiation or its reflection depends to a large extent on the particle size. A decrease in particle size also increases reflection. On the other hand, very small size would reduce efficiency too. This is reflected in **Table 3.8**.

Table 3.8:

Particle size	15 μ	6.0 μ	4.6 μ	3.2 μ	1.6 μ
Reflection	8%	10%	15%	20%	38%

(Courtesy : Fluorescent Lamps & Lighting by W. Elenbass).

It is estimated that about one third of 254 nm radiation is lost in the lamp. The light output increases with increase in the particle size. However, particle size above a



certain limit would again be detrimental. Hence an optimum size can be considered. The table 3.5 on particle size distribution shows that a maximum of 72% particles are in the range between 8 to 17 μ , considered to be an optimum one. It can be seen from the table that the lowly performing samples P-1 and P-3 have about 26% and 14% of their particles respectively beyond 17 μ size, which is much higher in comparison to others, which have less than 10% particles in that bracket.

Coming back to the wide range of variation in lumen output and its probable relation with coating thickness, one can calculate the absorption of radiation for different coating thickness. The intensity of absorption decreases according to the formula,

$$I_d = I_0 e^{-\alpha d},$$

where I_d = Intensity at penetration depth d .

I_0 = Intensity of impinging radiation

and α = absorption coefficient.

This formula would also hold true for the absorption of ultraviolet radiation in a phosphor coating. Although the grain structure of the coating causes a diffusion of rays and therefore an increase in the distance actually covered by them, diffusion effect has not been considered here. To get a good lamp efficiency, only a small percentage of the incident radiation i.e. 254 nm should be allowed to pass into the glass wall of the tube unabsorbed. An attempt has been made here to calculate the percentage of radiation remaining unabsorbed for different penetration depths of coating thickness.

In case of halophosphates, the absorption coefficient has been found to be around 1500 cm^{-1} , with the assumption that the particle size would be between 1-50 μ , which is indeed the case here. For a coating thickness i.e. penetration depth $d = 20\mu\text{m}$, the amount of unabsorbed radiation is about 5%, which reduces to 2.35% for $d = 25 \mu\text{m}$ and to about

1% for $d = 30 \mu\text{m}$. Thus the unabsorbed radiation, which is ultimately lost in the glass wall will increase with decrease in coating thickness, while for higher coating thickness, the visible light generated may be absorbed by the phosphor layer. Thus on both sides of the optimum coating thickness, there would be a marginal fall in the light output. However the range of variation is quite substantial and so other factors should be considered, these being.

(a) **The Mercury vapour pressure :**

If the mercury vapour pressure is too low, the probability of collision between electrons and mercury atoms also goes down, whereas excessive vapour pressure results in too much absorption of the resonance radiation. This would naturally have a bearing on the extent of emission of 254 nm and 185 nm radiation by the gas discharge. The effect of mercury vapour pressure on the intensity of light can be determined by varying the ambient temperature around the lamp. This is because a change in temperature will cause a change in vapour pressure. The results show that the maximum lumen output corresponds to an ambient temperature of about 25° C. The intensity falls off on both sides of this temperature. This result underlines the sensitivity of mercury vapour pressure to lumen output. The maximum efficiency corresponds to a vapour pressure of around 0.003 mm. The pressure of rare gas which is filled in the tube with mercury vapour is also important, although it is more relevant to the lamp starting process. The pressure also depends upon the current to certain extent.

(b) **The Tube dimensions :**

Among these the tube length assumes significance, as it decides the length of positive column, which emits light. There is an optimum value of diameter too, as a small diameter leads to high current density resulting in more excitation of higher energy levels. A larger diameter results into high absorption of the 254 nm radiation, due to the long

average distance to be travelled by the UV quanta before reaching the fluorescent powder coating. A larger diameter can also result into low vapour pressure.

Apart from the above factors, the quality of the phosphor also affects the performance. What it means here is the property and characteristic of the phosphor that creeps in during its preparation. Some of them are as under :

- The general experience with halophosphates show that phosphor compositions are preferably non-stoichiometric. [18] Maximum emission occurs at an overall metal/phosphorus ratio of 5/3 [19].

- The phosphor should be fired at a proper temperature. Lower temperatures might not initiate the process of solid state reactions or might not carry the process to the desirable level. On the other hand, higher temperatures may lead to undesirable phases and by-products, which adversely effect the efficiency. In short, the proper crystallinity of the material is a function of firing temperature. The energy transfer and thus the emission characteristics as well as the excitation characteristics being structure sensitive, this factor assumes importance. To maintain a proper atmosphere during the firing process is imperative. In certain cases, reducing atmosphere is needed and so phosphors fired in air give a lower efficiency. This is because the presence of air facilitates the formation of undesirable phases. The influence of H₂O and gases like NH₃ is also unfavourable [20].

Trace impurities like Aluminium, radium, iron, etc. also have an adverse effect on the efficiency of phosphors [19].

W. Elenbass enlists several parameters that decide the light output of the lamp per unit energy consumed. The relation between them is given by,

$$L = A \times B \times C \times D \times E \times F$$

where,

L is the lamp output per unit energy consumed given in lumens/watt.

A is the maximum luminous flux that can be produced by 1 watt = 680 lumens

B is the ratio of energy of emitted light quanta to that of absorbed light quanta (for 185 nm and 254 nm) = 0.44.

C is visual sensitivity which takes into account the capacity of human eye and the spectral characteristics of the phosphor. A value of 0.5 is agreed upon.

D is the quantum efficiency. A value of 0.85 has been considered here.

E is the efficiency of discharge to transform the applied power into resonance lines. A maximum value of 0.66 has been considered here.

F is the amount of UV radiation utilized. considering an absorption of 10% of the emitted light by the phosphor layer itself, this will be $100-10 = 90\%$ i.e. 0.9.

Hence, $L = 680 \times 0.44 \times 0.5 \times 0.85 \times 0.66 \times 0.9 = 76 \text{ lumens/watt}$.

This is perhaps the highest that can be achieved. At this rate the total lumen output of a 40W lamp amounts to 3040 lumens, which is much higher in comparison to around 2500 lumens that has been recorded.

The parameter A remains constant, while B has been calculated using the standard emission characteristics, which remain identical by and large. The parameter D giving quantum efficiency is also fairly reasonable. Hence the remaining parameters i.e. C, E and F come under scrutiny. Of these, parameter C would depend to a large extent on the emission characteristics. However in this case the emission characteristics have been found similar to the reported ones and the value of 0.5 has been calculated on that basis. Small differences would not effect the lumen output significantly. Parameter E is governed by electrical design conditions. One can expect that the maximum possible power is obtained and used but there is always some scope of loss here. However, it still does not account for the huge gap in the theoretical and practical values of lumen output.

This brings the discussion to parameter F, which depends on the absorption of UV radiation by the phosphor and also the absorption of visible light by the phosphor. It has been already mentioned that about one third of the reflected 254 nm radiation is lost in the

lamp. But the reflection increases with decrease in particle size (Table 3.8). Hence the overall absorption would depend upon the amount reflected. Thus the factors, particle size and coating thickness again become relevant here. In this context i.e. with reference to table 3.8, it would be appropriate to mention that a lamp made with 15 μ fraction may be expected to give about 10% more light than a lamp coated with the phosphor of 1.6 μ particle size.

The total efficiency η of a phosphor can be expressed by,

$$\eta = \eta_{qe} \frac{\lambda_{ex}}{\lambda_{em}}$$

Taking an average Q.E of 0.85 and λ excitation = 254 nm, the calculation must be done for both emission lines, i.e. 475 nm and 555 nm.

Thus,

$$\eta = 0.45 \text{ and } 0.39 \text{ respectively.}$$

Taking simple average

$$\eta = 0.42.$$

This will however be higher, as the 475 nm peak is stronger. Taking the efficiency of the electrical apparatus into consideration, the overall efficiency would be

$$E = 0.42 \times 0.66 \text{ (considering maximum energy conversion from electrical to UV by the discharge).}$$

$$\therefore E = 0.28$$

Thus an overall efficiency of 28% is obtained for the fluorescent lamp i.e about 12 watts power is utilized out of 40 watts. This is still much higher than the incandescent

lamp. However the particle size and the average lumen output are subject of controversies since some Japanese manufacturers have claimed that a 3-5 micron particle size gives more lumen output. Not much literature is available on this aspect.

Colour Rendition Characteristics :

The colour rendition characteristics of a light source depends on the visual characteristics of human eye and the spectral characteristics of the emitted radiation. It is widely known that the human eye does not have the same sensitivity for all wavelengths in the visible region. The sensitivity is maximum for the wavelength 555 nm and decreases on both sides of this wavelength along the visible spectrum. This sensitivity curve remains constant. The variable factor is the spectral characteristic, which may vary from source to source. A source having emission centred around 555 nm would be ideal as it is centred around the maximum sensitivity region. The overall colour effect would thus depend upon the spectral characteristics of the light emission and can be described in terms of two different parameters namely, colour coordinates and colour rendition index. Both these parameters provide a measure of proximity of the emitted radiation to the ideal white colour that is desirable for tubular fluorescent lamps.

Table 3.9 gives the colour coordinates of the phosphor samples, along with the range of variation of colour coordinates for the five lamps. The average value of x and y coordinates move in a narrow range and the range of variation is also identical for all the samples. In general, it has been observed that for higher lumens, the colour coordinates also shift slightly to the higher side. However the position of the colour points will be better indicated by a chromaticity diagram. As the colour points move in a narrow range, a small section has been considered in the chromaticity diagram. This is given in **Fig. 3I**. Figure shows that the values of x-coordinate move in a narrow range compared to the y-coordinate which are more spread out. The general trend seen so far is almost maintained as the samples with higher lumen output have higher y-coordinates.

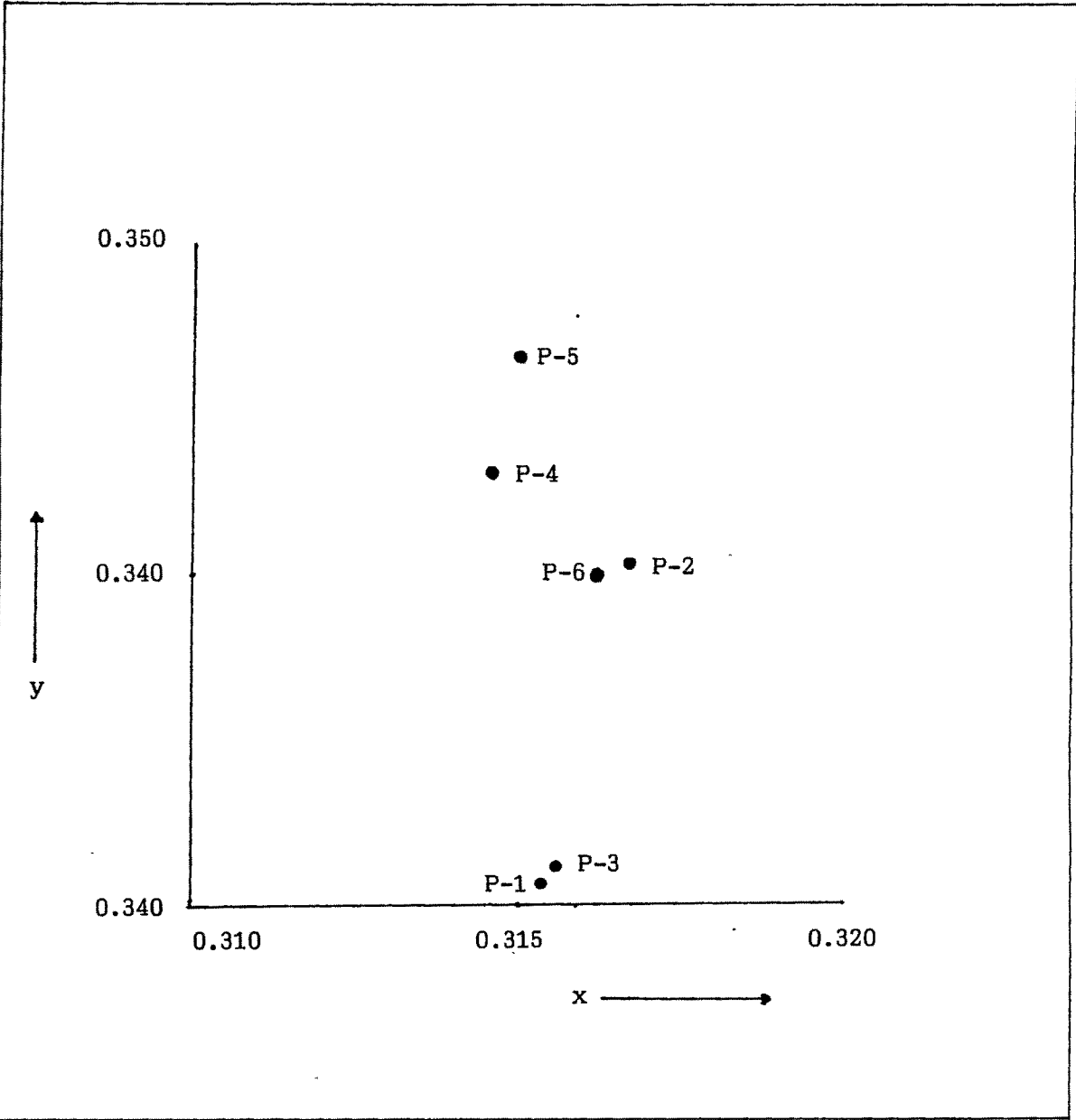


Fig. 3I : Section of chromaticity diagram showing average colour points of the Lamp samples.

Table 3.9 :

Sample	Average value of corodinales		Range of variation	
	X	Y	X	Y
P-1	0.3154	0.3404	0.314 to 0.317	0.340 to 0.341
P-2	0.3168	0.3452	0.315 to 0.318	0.344 to 0.346
P-3	0.3156	0.3406	0.314 to 0.317	0.340 to 0.342
P-4	0.3146	0.3466	0.314 to 0.317	0.345 to 0.349
P-5	0.3150	0.3484	0.315 to 0.318	0.346 to 0.349
P-6	0.3162	0.3450	0.314 to 0.319	0.344 to 0.346

It is also possible to find out the colour coordinates using the data on spectral sensitivity of human eye, from the emission spectrum of the phosphor. The data on the spectral sensitivity of human eye to red, green and blue colours is available for segments of 10nm from 390 nm to 700 nm. But this type of calculation becomes tedious as the emission spectrum has to be also broken up into segments of 10 nm to determine the intensity of each segments. This being inconvenient, another method has been adopted. The emission spectra i.e. the spectral characteristic of the sample was superposed on the eye sensitivity curves for the three colour regions. The area under the curve was calculated for each of them. This is given in Fig. 3J. On doing so it was found that the area under the curves $x(\lambda)$, $y(\lambda)$ and $z(\lambda)$ was around 32 %, 39% and 29% respectively.

Thus the x and y coordinates would be 0.320 and 0.390 respectively. However, the emission of mercury gas has to be also taken into consideration, which accounts for about 10% of the light on an average. Most of this is in the violet-blue region (about 50%) while the rest is spread out in the green and yellow regions evenly. Taking these into account, the revised value of x and y coordinates would be around 0.315 and 0.375

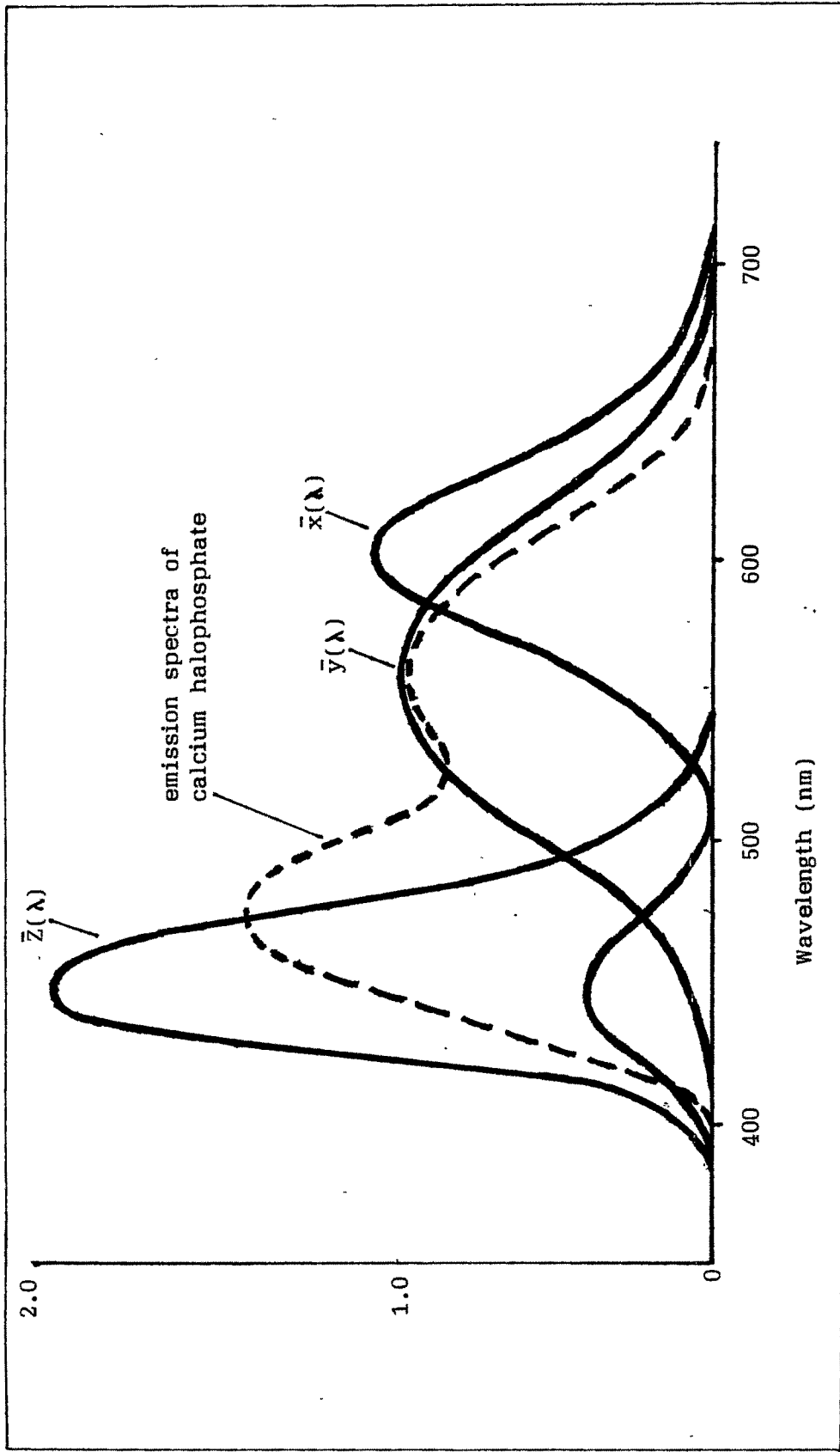


Fig. 3J : The C.I.E. colour matching functions for standard observer (bold lines). Broken line shows the spectral characteristics of the phosphor sample.

respectively. In calculating the above, the emission characteristics of sample P-4 has been taken. The experimental and theoretical value of x and y coordinates are given below.

	<u>Coordinates</u>	
	'x'	'y'
Experimental	0.3146	0.3466
Theoretical	0.3150	0.3750

It can be seen that the theoretical value is a bit higher than the experimental values, the difference being more in case of y coordinate compared to the x coordinate. There is a possibility of absorption of the emitted radiation in the visible region by the phosphor layer. It may be at a selective wavelength i.e. only a particular wavelength may be absorbed. This is one of the reason, why there can be a difference between the calculated and observed values. However, it has to be considered that a precise value of colour coordinates is difficult to predict theoretically. The values of these coordinates correspond to the different categories of fluorescent lamps viz. cool daylight, warm white, deluxe, etc. Hence a better measure of the distribution of spectral energy over the visible spectrum is the value of colour rendering index.

The calculation of the colour rendering index is again a long drawn procedure. It involves the measurement of chromaticity coordinates of eight standard samples under a standard reference source and the test source. In the deficiency of such standard samples and sources, a measurement of the CRI is almost ruled out. Fortunately, some literature provides the data relating the colour coordinates to CRI and the corresponding colour temperature. The expected value of CRI from such a data sheet is given in **Table 3.10**.

Table 3.10 :

<u>Sr. No</u>	<u>Chromaticity coords</u>		<u>Correlated colour</u>	<u>CRI</u>
	<u>x</u>	<u>y</u>	<u>temperature</u> ° K	
1.	0.3131	0.3371	6430	76
2.	0.3138	0.3452	6350	72
3	0.3721	0.3751	4230	64
4	0.3779	0.3882	4150	59
5	0.4091	0.3941	3450	57
6	0.4402	0.4031	2940	51

[Courtesy : Measuring colour - R.W.G. Hunt, Ellis Horward Ltd., 1987, page no 189, app. 5.3]

The phosphor samples studied have coordinates nearest to that given by values at serial no. 2 i.e. 0.3138 and 0.3452, which corresponds to a colour temperature of about 6350° K and a CRI value 72. The value of CRI is a bit low and this is expected in view of the fact that the emission is concentrated more in the blue and green region and lacks in red component.

TSL - EPR STUDY OF COMMERCIAL LAMP PHOSPHORS :

An ordinary fluorescent lamp is coated with a phosphor material inside the shell. The coating is of few microns in thickness. This coating is being continuously hit by particles generated due to the gas discharge, while the tube is on. These particles may be electrons or ions of mercury and other inert gas filled in the tube to trigger ignition. The phosphor material being crystalline in nature, the incident radiations of particles are likely to create defects in the phosphor material. Defects can play an important role in influencing the electrical, thermal, optical and magnetic properties of the solids [21,22]. The performance of the phosphor is based on its optical properties and any significant change in its optical properties can adversely affect its performance. Hence it may be safely assumed that a good phosphor material should not show any appreciable shift in its optical properties. However, it remains to be proposed, as to how this factor can be investigated. It also remains to be mentioned that apart from electrons and ions, the ultra violet photons generated by the discharge can also cause defects. Hence, investigations have been carried out using gamma rays as well as ultraviolet rays for the purpose of irradiating the phosphor material.

Various defects are formed due to incidence of radiation on the solids. One of them is the F-centre, in which an electron is trapped in an anion vacancy [23] while the U-centre is a H⁻ ion substitution for halogen ion [24], V-centres are impurity stabilized hole centres [25]. Irradiation in oxides also produces large macroscopic defects such as dislocation loops and voids [26]. Dislocations are also produced in electron irradiated alkali halides [27].

The Antimony and Manganese doped in the halophosphates take the position of the alkali metals as substitutional ions in the lattice. Under the influence of the crystal field, there is splitting of energy levels of these ions. Transition of electrons between the vibrational/rotational levels of different electronic states [i.e. ground state \rightarrow excited state

and excited state \rightarrow ground state] gives rise to the emission of fluorescence. The transition probabilities also depend upon the availability of these energy levels.

Irradiation results into alteration at different sites of the crystal viz. creation of voids, trapping of electrons and holes, aggregation of ions, etc. If these sites involve the Antimony and Manganese ions, which are the fluorescence centres by virtue of their energy level distribution, then an additional electron, or hole, or the aggregation of such dopant ions may lead to a change in the crystal field in the vicinity of the fluorescence centre. This change in the crystal field may subsequently lead to a redistribution of energy levels. The transition probabilities may also change resulting into a lower probability for the desired transition and thus lower efficiency of absorption and emission. Thus a dopant, which is supposed to be a fluorescence centre is reduced to a trap, which stores energy but ceases to be a fluorescence centre. It can be liberated only by thermal stimulation. However the exact TSL centres can be known only by a joint TSL-EPR study. TSL by itself cannot reflect upon the nature of radicals responsible for a particular glow peak, but a combination of TSL-EPR can.

Putting in other words, the periodic function of the lattice coupled with the wave function of a free electron, when solved quantum mechanically permits only specific values for electron energies in the solids [28]. Imperfections in a crystal gives rise to localised energy states; an electron associated with the imperfection having energy level that is forbidden in a perfect crystal. Local deviation from the periodic potential of the perfect crystal gives rise to localised energy states characterised by wave functions that decay exponentially in amplitude with distance from the imperfection site. When considered with respect to the energy bands, these localised levels normally lie in the forbidden gap. Prominent imperfections are impurities, vacancies, interstitials, or complex imperfections formed by the aggregate of the simple imperfections. Localised levels can also be directly associated with the impurity itself and correspond to atomic levels of the impurity as altered by the dielectric constant and interaction of the crystal [29]. Such levels are additional levels, which are not at all present in the chemically pure crystal. These

additional levels may adversely affect the fluorescence emission, if the impurity in question is the dopant and the codopant. Hence it is desirable that there is no involvement of the dopants and codopants in the TSL mechanism. This can be confirmed only if the glow peaks are due to radicals other than the dopants and codopants i.e. Sb and Mn. Hence the TSL study has to be supplemented by EPR investigation.

Almost no literature is available on the TSL of lamp phosphors. This is most probably so, as TSL study is not of direct consequence or does not lead to any significant parameter measurement of lamp phosphor. The only study of TSL in lamp phosphor [30] available suggests its possible use as TLD. The dose rate --- TL intensity relation has been found to be linear but the sensitivity will be nowhere near the LiF or CaSO₄ based TLD's. However the study under consideration presents a different angle. It will supplement the investigation on the suitability of a material as phosphor.

The subsequent pages give the result of TSL by gamma and UV irradiation, TSL spectra and ESR investigations on alkali halophosphates doped with antimony and manganese.

Thermally Stimulated Luminescence by gamma irradiation :

All the six samples of commercial lamp phosphors were irradiated by a gamma dose of 15 gray per minute for 3 hours (Total dose - 2.7 k Gy). The samples were heated from room temperature to 673° K at a linear heating rate of 6° K/sec. Most of the phosphors exhibited three peaks. All the glow curves are presented in Figs. 3K - I to 3K : VI and also tabulated in Table 3.11.

Figure 3K - I shows the glow curve for sample P-1. There are three distinct peaks around 378°K, 453°K and 548°K. Glow curve for sample P-2 in fig. 3K - II shows distinct peaks at 393°K and 573° K while a small peak is seen at around 483° K. Glow curve in fig. 3K - III for sample P-3 again shows three distinct peaks around 383° K, 453° K and 548°K. In case of sample P-4 in fig. 3K - IV, the glow curve has two clear peaks at 358°

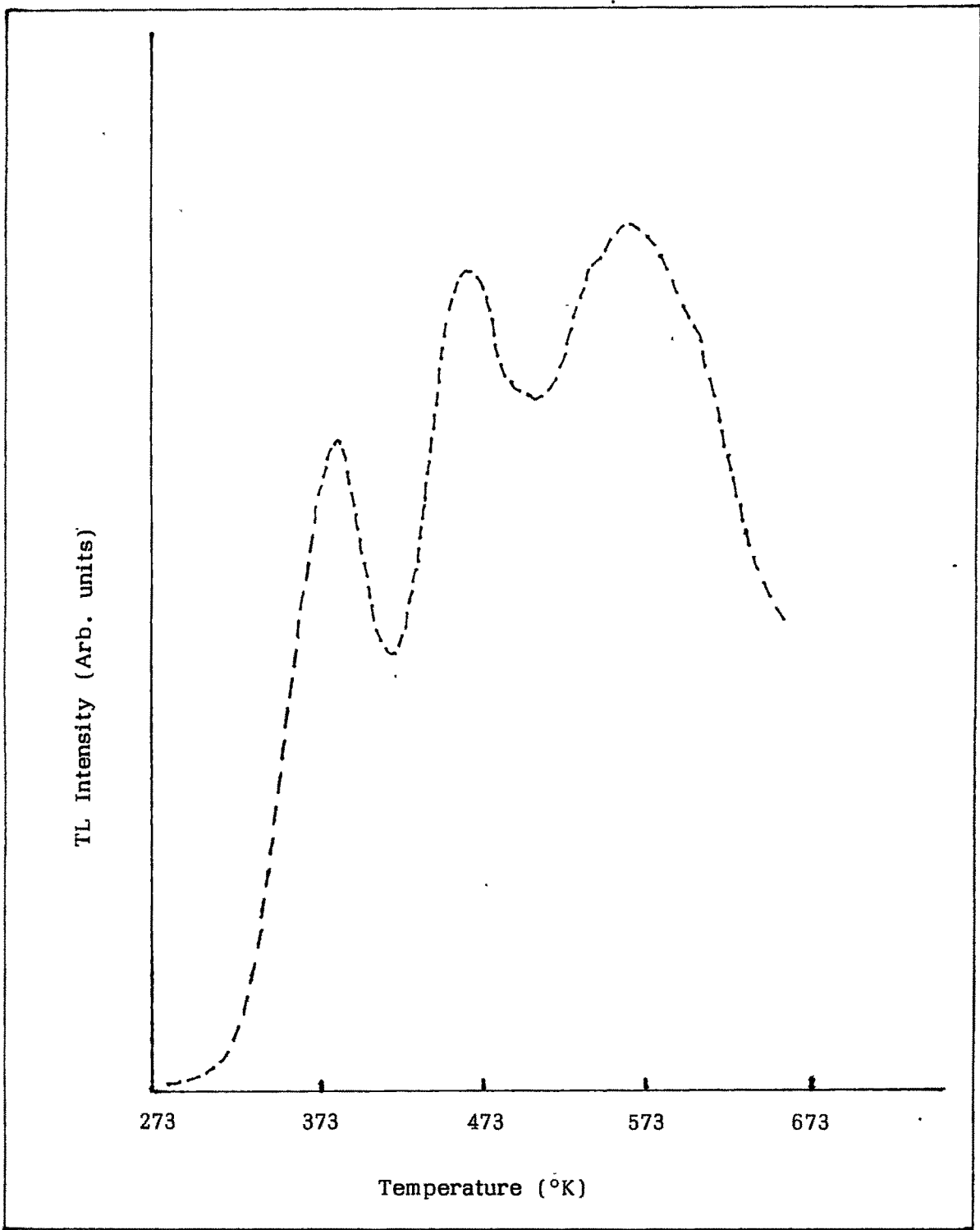


Fig. 3K-I : TSL glow curve (gamma irradiated) for sample P-1.

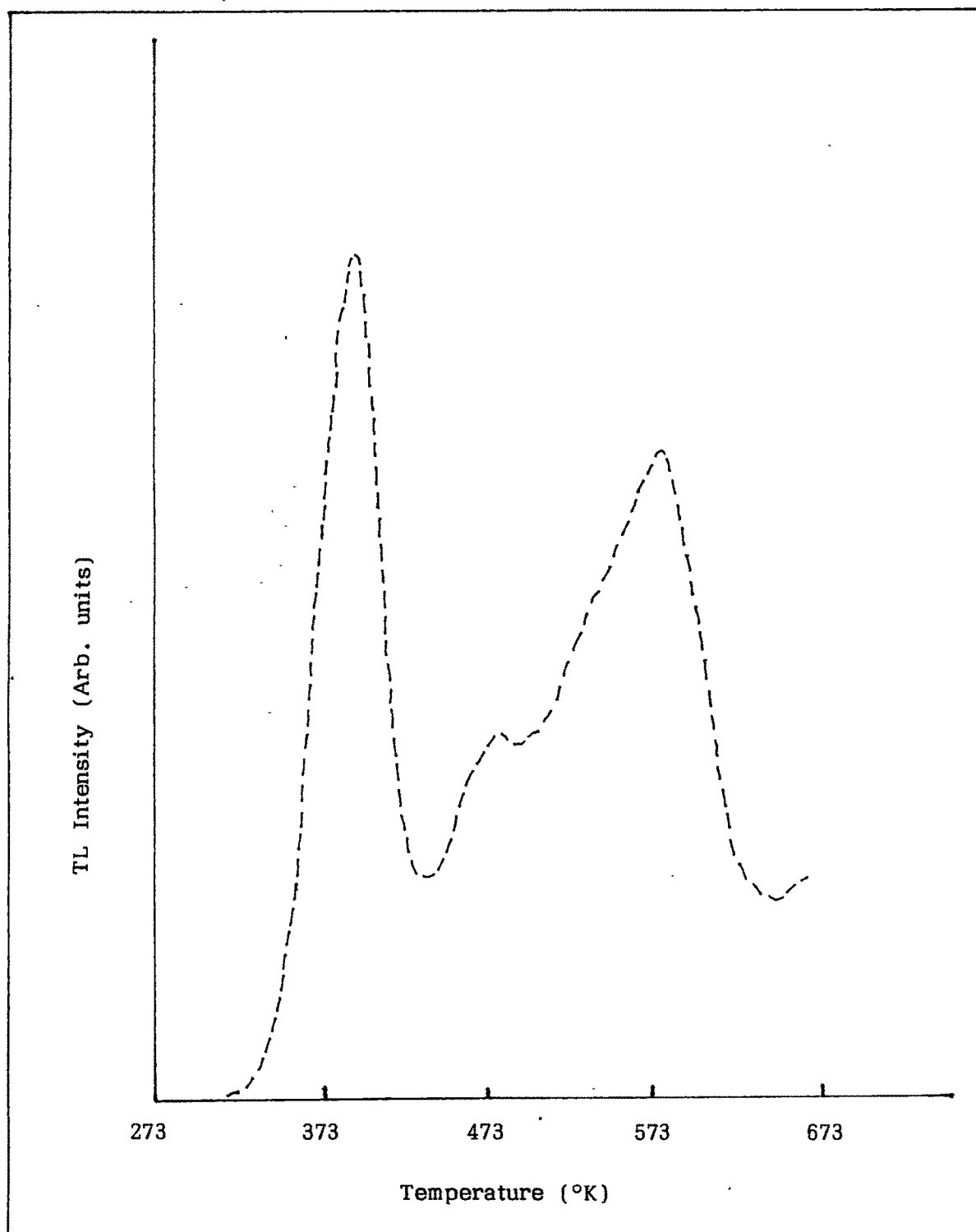


Fig. 3K-II : TSL glow curve (gamma irradiated) for sample P-2.

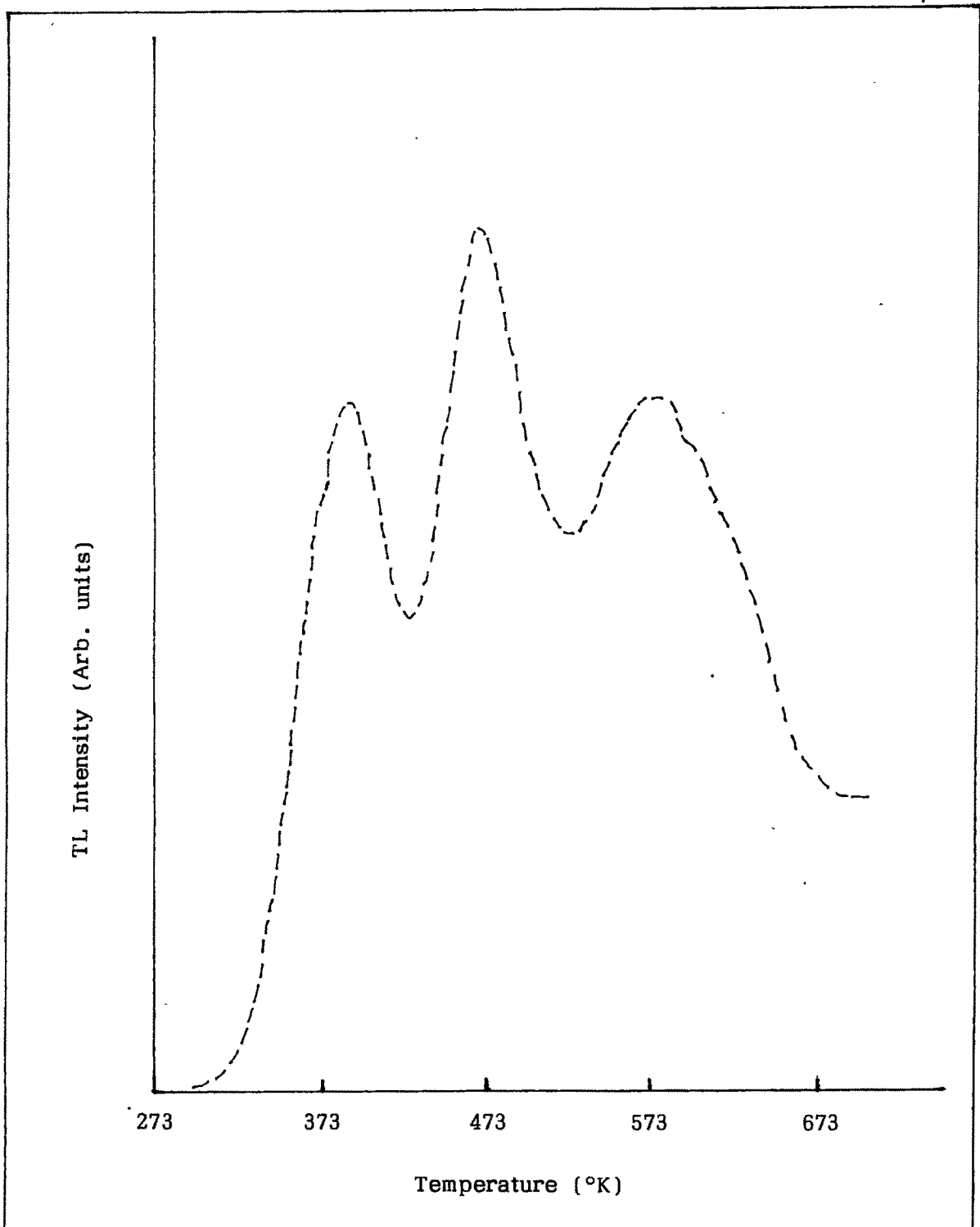


Fig. 3K-III : TSL glow curve (gamma irradiated) for sample P-3.

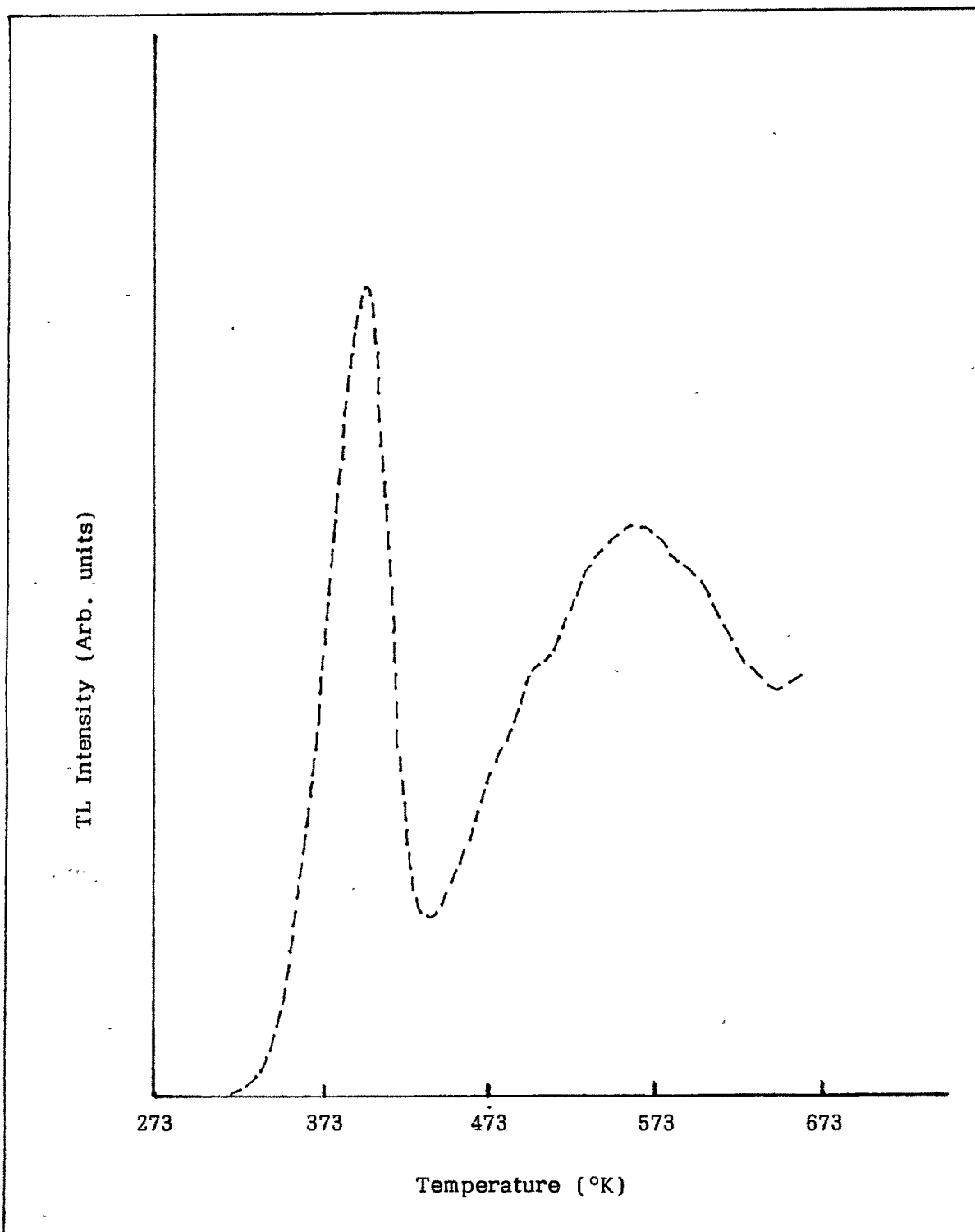


Fig. 3K-IV : TSL glow curve (gamma irradiated) for sample P-4.

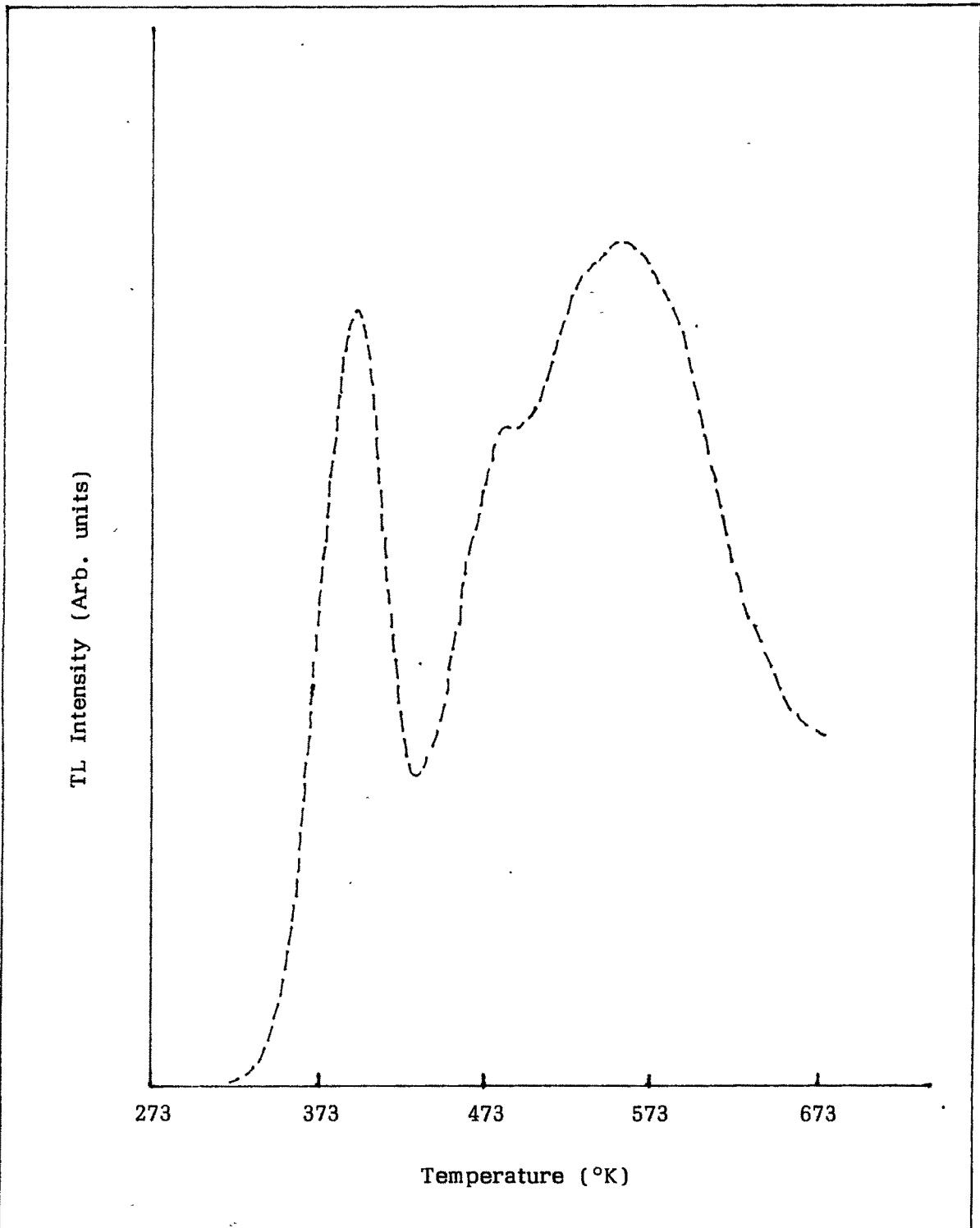


Fig. 3K-V : TSL glow curve (gamma irradiated) for sample P-5.

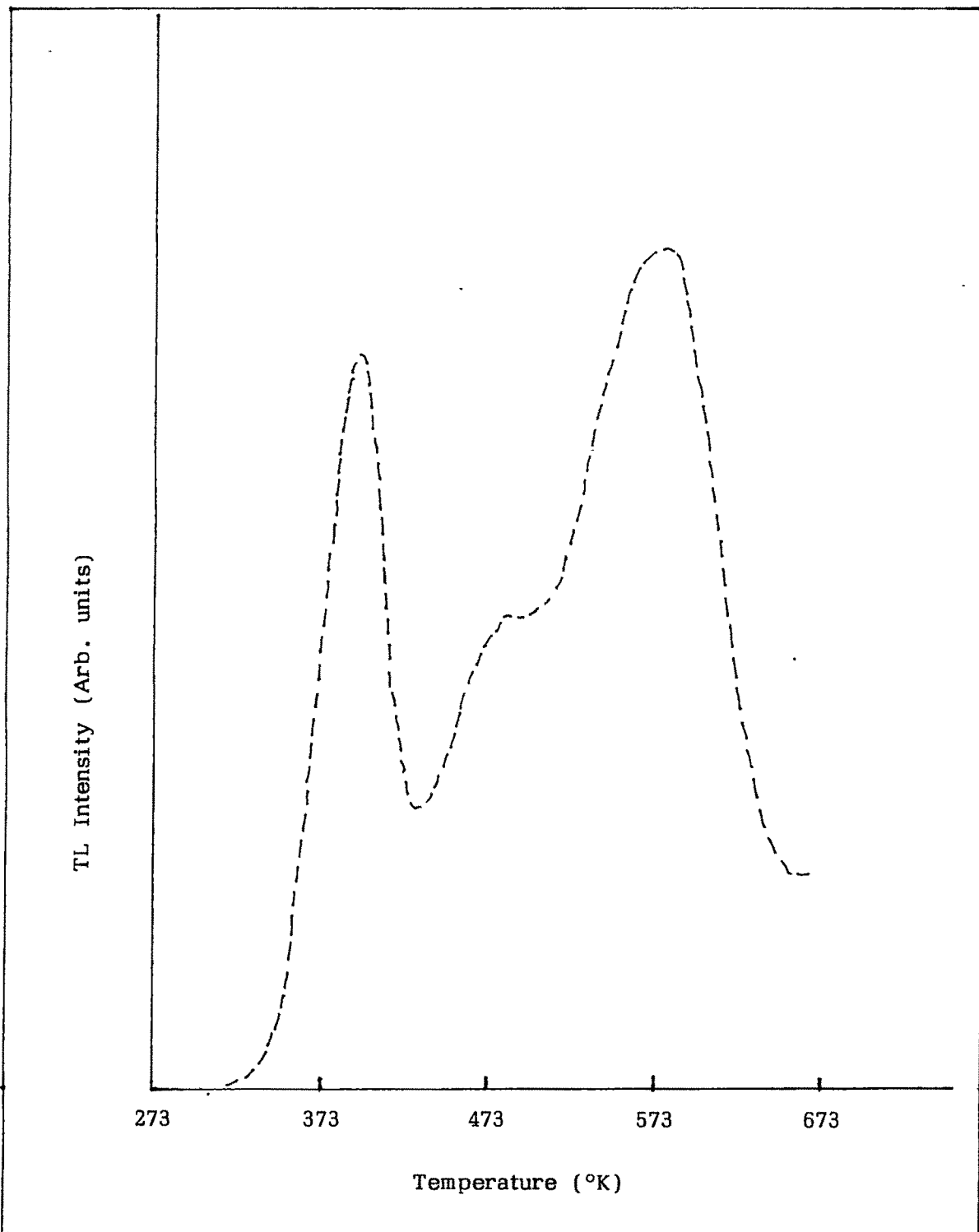


Fig. 3K-VI : TSL glow curve (gamma irradiated) for sample P-6.

K and around 553° K. A slight lamp can be seen around 503° K. The glow curve of sample P-5 in fig. 3K - V once again exhibits two peaks at 398° K and around 543° K clearly, while there is a small peak around 473° K. Sample P-6 has peaks around 393° K and 563° K and a small one around 493° K. This is shown in the glow curve in fig. 3K - VI.

As it can be seen from the figures, the first peak is quite well defined in all the cases, while the other major peaks are a bit spread out. Sample P-1 and P-3 display three clear peaks, while samples P-2, P-5 and P-6 have two clear peaks, with the second one being a small peak. Sample P-4 has only two clear peaks, with a slight hump.

An attempt has been made to find the values of trap depth, for each of the peaks. Since the readings have been taken for a single rate, empirical methods have been adopted to find the activation energies. Here, it needs to be mentioned again that the aim of the study is to find the radicals responsible for the respective peaks. Not much has been reported about the TSL of lamp phosphors, but there has been some work on chloroapatites. The empirical methods are first approximations for the evaluation of activation energies, where an idea of the value of frequency factor, 's' is the pre-requisite. Based on the value of 's' for chloroapatites in reported works [31], one of such empirical method suggested by Urbach [32] has been employed here to find the activation energies. The values are listed in **Table No. 3.11** for samples P-1 to P-6

It can be seen from the table that the first peak is centred around 0.78 eV with a range of variation of about 0.04 eV. The range of variation for the second peak is about 0.1 eV, which is quite high, compared to the first peak. The second peak averages around 0.946 eV. The third peak average around 1.11 eV and has a range of variation of 0.06 eV.

Table 3.11 :

<u>Sample</u>	<u>Peak Temperatures [T_m(oK)]</u>	<u>Activation Energy [E(ev)]</u>
P - 1	378° K	0.756 eV
	453° K	0.906 eV
	548° K	1.096 eV
P - 2	393° K	0.786 eV
	483° K	0.966 eV
	573° K	1.146 eV
P - 3	383° K	0.766 eV
	453° K	0.906 eV
	548° K	1 096 eV
P - 4	398° K	0.796 eV
	* 503° K	1.006 eV
	553° K	1 106 eV
P - 5	398° K	0.796 eV
	473° K	0.946 eV
	543° K	1.086 eV
P - 6	393° K	0.786 eV
	493° K	0.986 eV
	563° K	1.126 eV

* Slight hump.

For the first and third peaks, the range of variation of the activation energy is very low, which hints the possibility of the same radical being responsible for the peaks in all specimens. However, this cannot be said conclusively only on the basis of the TSL results. Looking to the comparatively wider range of variation for the second peak, the possibilities remain open.

The glow curves were recorded on a 'Nucleonix' make TL set up interfaced with a PC-486.

TSL Spectrum :

The TSL spectrum of all the samples were taken on an apparatus designed for the purpose. It has a monochromator which is operated by a motor. Heating was controlled by a dimmerstat. The data is fed to the PC-486 through the 'Nucleonix' make TSL set up.

TSL spectrum of the samples were taken for each of the peaks or humps. The wavelength range scanned was between 350 nm and 700 nm.

The results exhibited by all the phosphors show a general trend. Spectrum taken at three different temperatures for the three different peaks show two peaks in all the six samples. One of the peak remains around 410 nm, while the other around 550 nm. In some samples, there is a small variation in the wavelengths of the peaks at different temperatures. Another common factor observed is the increase in intensity of the first peak, while a decrease in intensity of the second peak with rise in temperature. The increase in intensity of the first peak was found to be substantial. Compared to this, the decrease in intensity of the second peak was quite small. One of the sample is however an exception to this trend. The individual results are presented as follows.

Sample P-1 shows a relatively low intensity peak at 400 nm for the first peak of the glow curve i.e. 378° K. The second peak of the spectrum is at 550 nm and is more intense. For the 453° K glow curve peak, intensity of the 410 nm spectrum peak is more

than that of 550 nm. The difference in intensity between the spectrum peaks increases for the third glow curve peak at 548° K. The spectrum is given in **Fig. 3K¹ - I**.

The spectrum in **Fig. 3K¹ - II** for sample P-2 shows a single peak at 550 nm for the glow curve peak at temperature 393° K. For the subsequent peaks at temperature 483° K and 573° K, the spectrum shows another peak at 410 nm with increasing intensity, while the intensity of the 550 nm peak decreases slightly

Spectrum of sample P-3 in **Fig. 3K¹ - III** follows the same characteristic as the previous two. While the second peak remains steady with small variation in intensity with temperature, this sample shows variation in the wave length of the first spectrum peaks, the first at 415 nm, second at 380 nm and the third at 420 nm.

The spectrum of sample P-4 in **Fig. 3K¹ -IV** again exhibits a single peak at 550 nm for the glow curve peak at 398° K. This sample is markedly different from the others as it exhibits only a single spectrum peak for each of the glow curve peaks. The peak at 550 nm is absent for the successive temperatures at 503° K and 553° K. The peak at 410 nm gains in intensity with temperature.

Sample P-5 again goes by the general trend with a small peak at 420 nm and another intense peak at 545 nm for the first glow curve peak at 398° K. For the subsequent temperatures at 473° K and 543° K, the peak at 420 nm increases in intensity while the intensity of the other peak remains almost the same with a slight decrease. There is also a very minor shift in the wavelength of the second peak. The results are shown in **Fig. 3K¹ -V**.

Fig. 3K¹ - VI gives the results for sample P-6, which are along the same line. The first peak lies around 410 nm, but varies a bit with increase in temperature. The wave length of the second peak decreases with the successive temperatures i.e. 393° K, 493° K, 563° K.

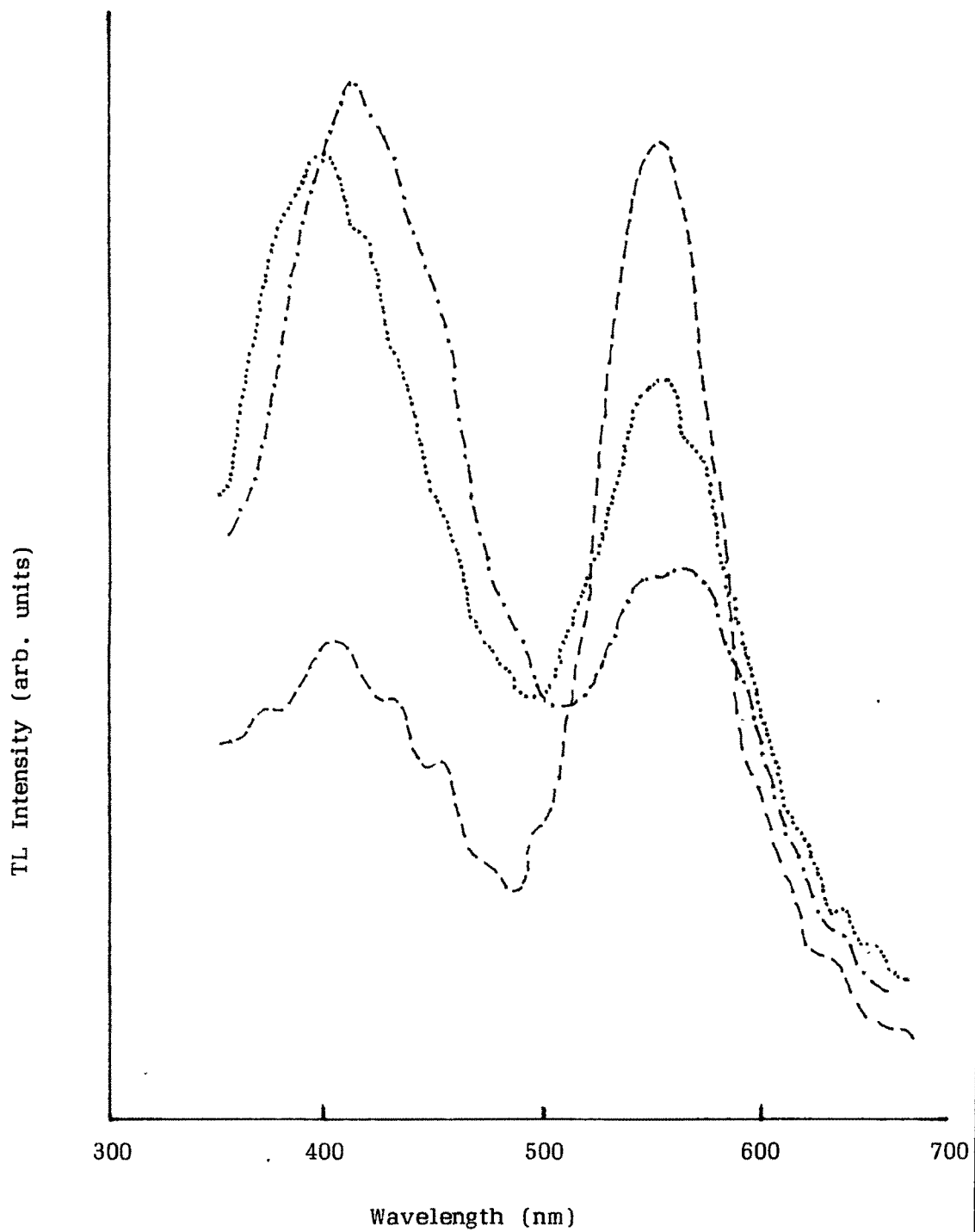


Fig. 3K'-I : Spectrum of sample P-1 for temperatures corresponding to peak 1 (-----) peak 2/hump (.....) and peak 3 (-.-.-.-).

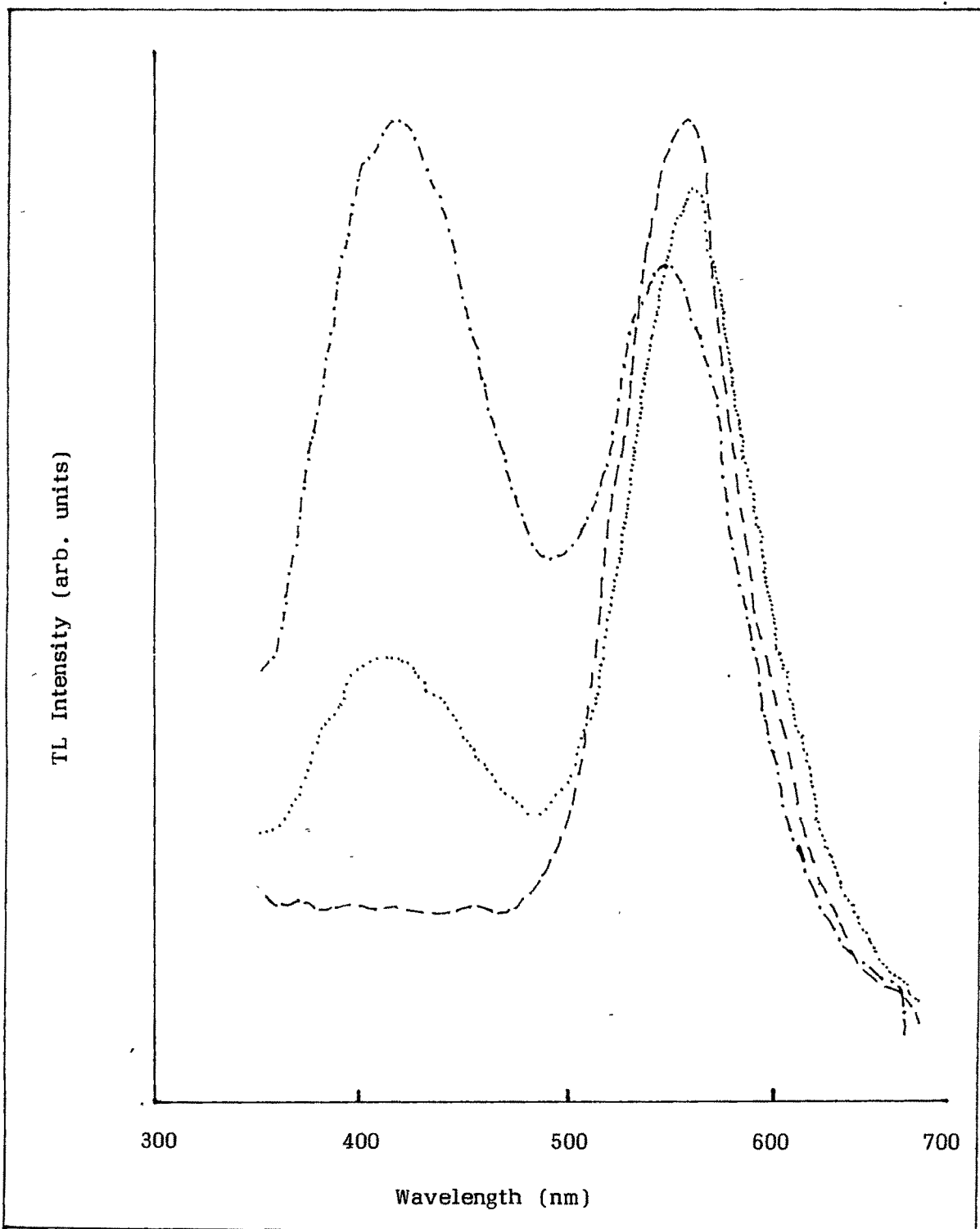


Fig. 3K'-II : Spectrum of sample P-2 for temperatures corresponding to peak 1 (-----) peak 2/hump (.....) and peak 3 (-.-.-.-.).

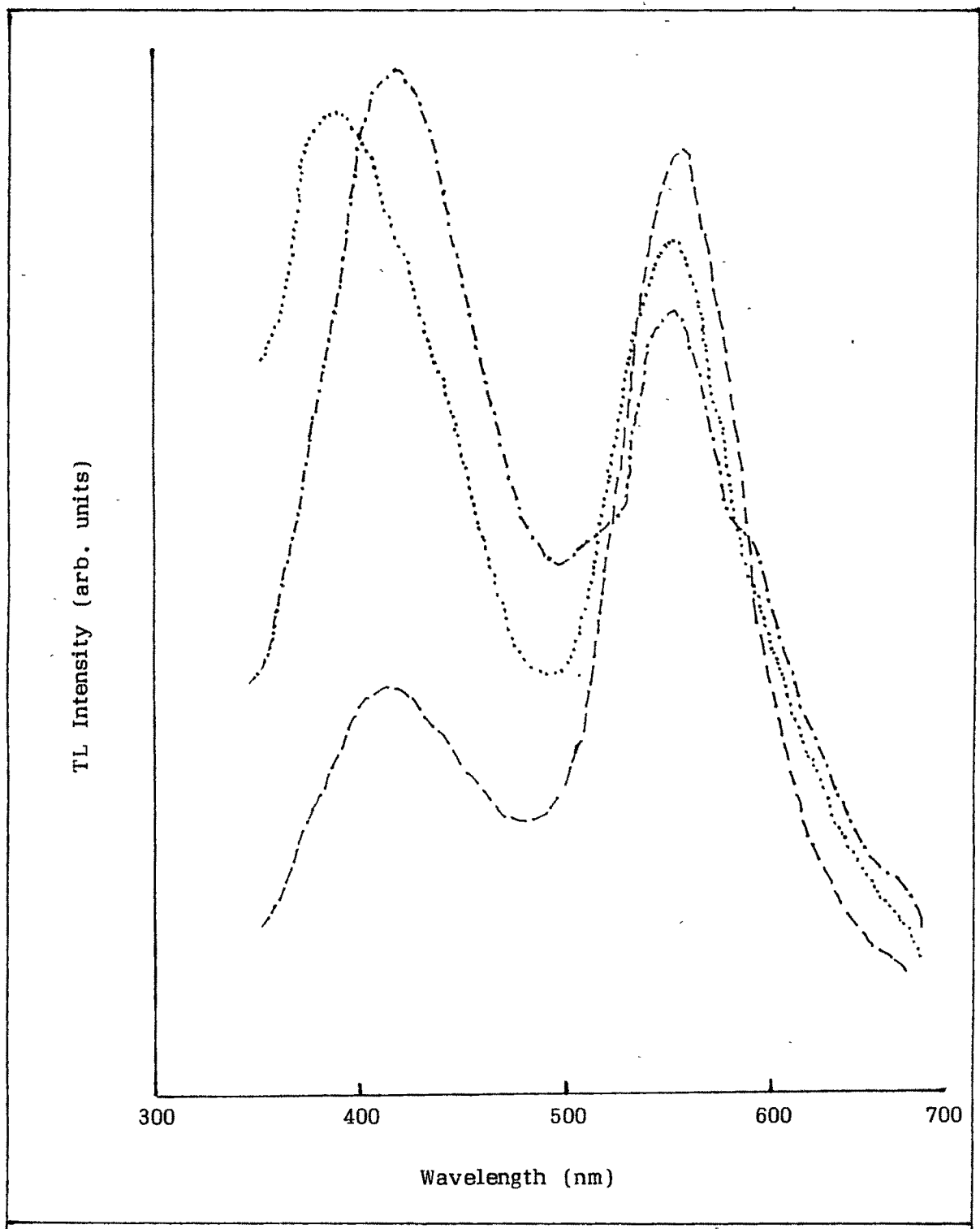


Fig. 3K'-III : Spectrum of sample P-3 for temperatures corresponding to peak 1 (-----) peak 2/hump (.....) and peak 3 (-.-.-.-.).

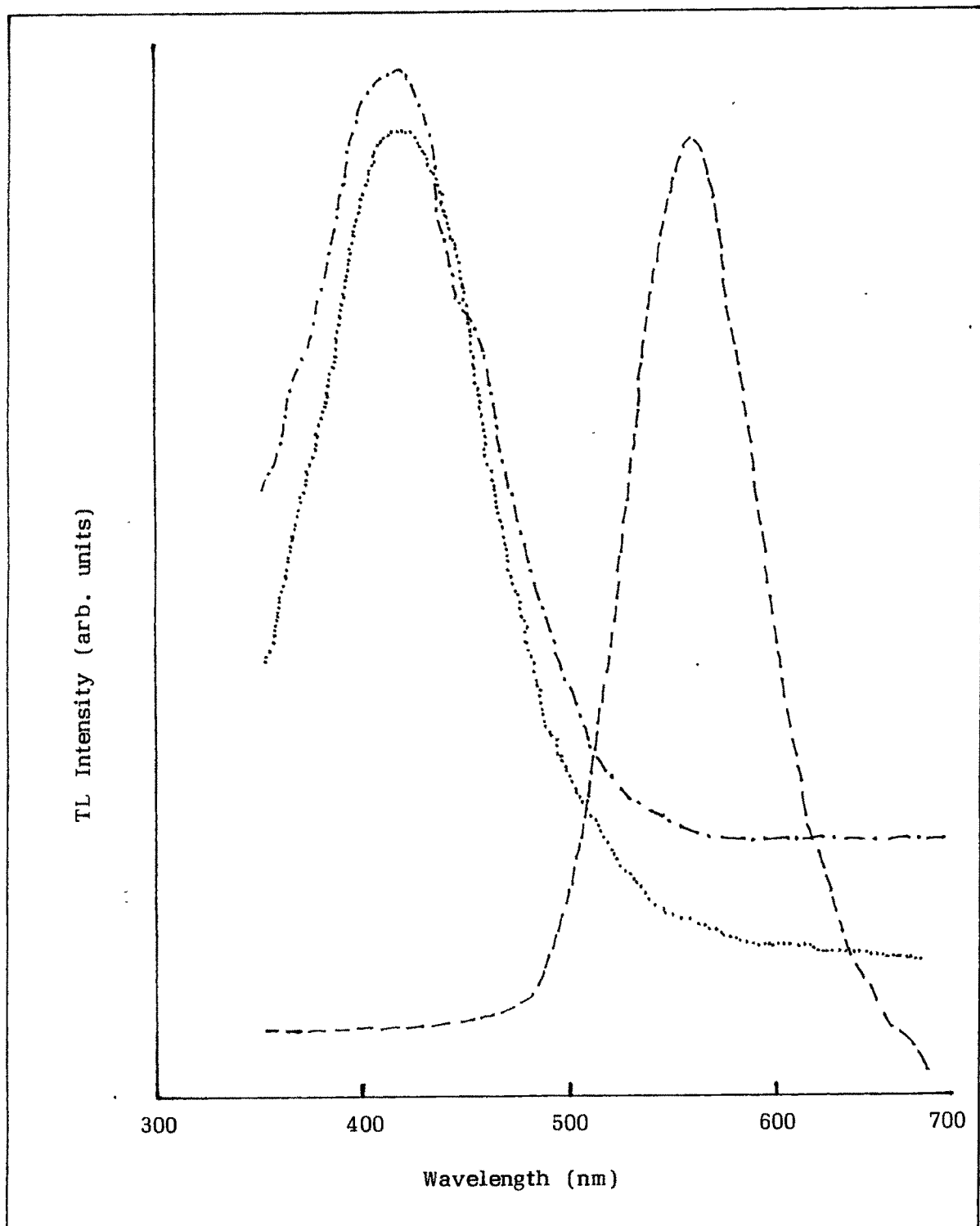


Fig. 3K'-IV : Spectrum of sample P-4 for temperatures corresponding to peak 1 (-----) peak 2/hump (.....) and peak 3 (-.-.-.-).

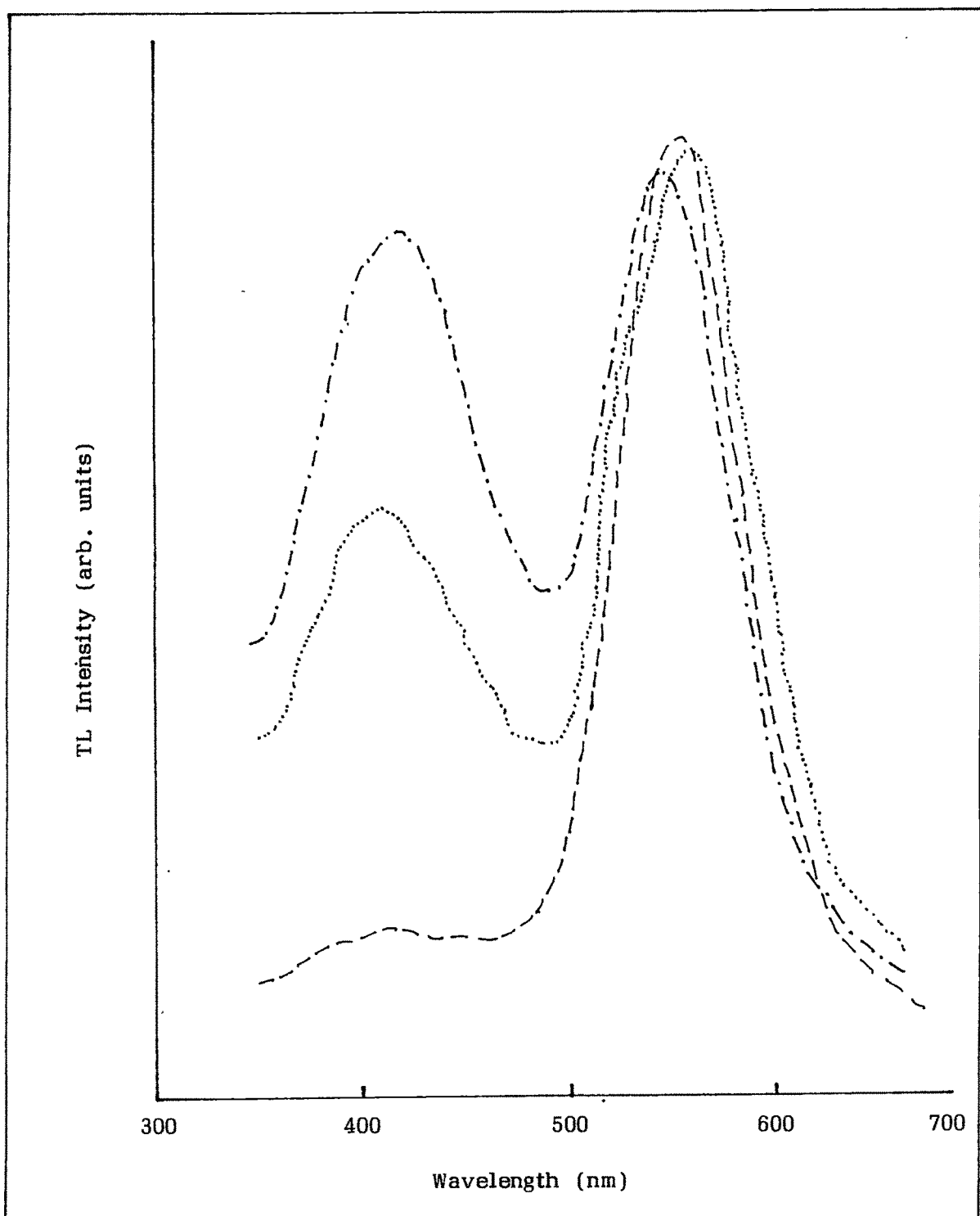


Fig. 3K'-V : Spectrum of sample P-5 for temperatures corresponding to peak 1 (-----) peak 2/hump (.....) and peak 3 (-.-.-.-).

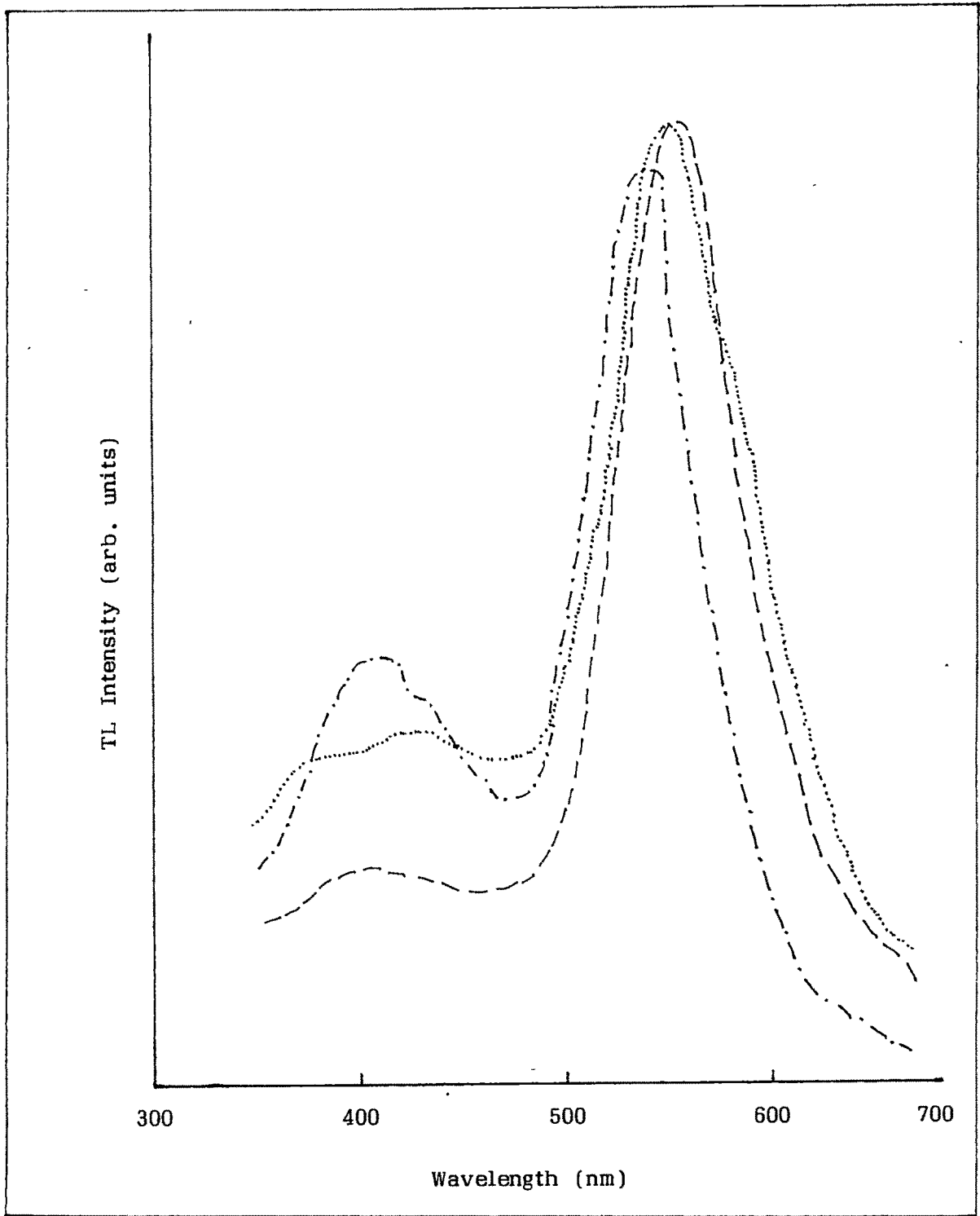


Fig. 3K'-VI : Spectrum of sample P-6 for temperatures corresponding to peak 1 (-----) peak 2/hump (.....) and peak 3 (-.-.-.-).

Taking a review of the glow curves, it becomes obvious that there are three peaks in general, with the only exception of sample P-4, in which the second peak can be hardly described as a hump. Corresponding results of the TSL spectrum almost support this. These three general peaks of the glow curves can be associated with three different impurities or traps, but not necessarily. The spectrum does not exhibit three different peaks for the respective glow peaks, but only two. This suggests that two of the three trap levels contribute to a single spectrum peak. Results of sample P-4 puts some light on this. It may be suggested from the results of this sample that the trap level associated with the first glow peak contributes heavily to the 550 nm spectrum peak. This is confirmed by the results, in general too. Analysing the results of P-4, further, it may be suggested that form the TSL spectrum peak around 410 nm is associated with the trap level responsible for peaks at the two higher temperatures.

Comparison of the Quantum efficiency results with the TSL spectrum becomes interesting. On the basis of Q E results, the samples can be placed in the following order of performance.

P-4, P-2, P-5, P-6, P-1, P-3.

The above trend has an interesting following in case of TSL spectrum results. The first spectrum peak is absent in case of samples P-4 and P-2 for the glow peak at lowest temperature. For the subsequent samples i.e. P-5 and P-6 in the order, this spectrum peak is only a small hump, but in the last two samples P-1 and P-3, they are well defined

The existence of single peaks at the three subsequent temperatures in case of sample P-4 may be attributed to a higher degree of crystallinity. From over all results normally one can say that there is a similarity between the fluorescence spectra of the samples and the TSL spectra. Both have two peaks in general. The second peak especially, almost coincide with each other, but the first peak differs substantially. However this is absolutely misleading, as both these results are due to entirely different phenomena, one fluorescence and the other thermoluminescence. The results of fluorescence spectra may give an idea of the relative quantity of dopants on the basis of

the relative peak intensities. It has been seen that the relative quantities of the dopants do not vary much from sample to sample. Had these variation been substantial and/on the exact amount of dopants known, it could have been easier to correlate these dopants to the peaks of TSL spectra. But here, it will indeed be difficult to comment whether the peaks are related to the defects involving the dopants or to the host matrix. The answer can be found with the help of EPR spectroscopy, which is discussed later in this chapter.

TSL by UV irradiation :

The phosphor coating is also bombarded by the UV photons, which are generated by the low pressure mercury discharge. Having a wavelength of 253.7 nm, they have an energy of 48.9 eV, compared to that of γ - rays, which have an energy of 1.17 MeV. The results have been also found to be different from the gamma irradiated TSL results.

For UV irradiation, the samples were exposed to radiation from a quarter pen ray UV lamp giving an output of 1.343 J/m² of 253.7 nm UV rays at 15 cms, for 1 hour

The results in **Figs. 3L - I to 3L - VI** show that only one peak has been found in the glow curve. The sample were heated up to 573° K. The rise at the higher temperature end is attributed to the IR signal and not TSL signal. In this case too, the trend observed earlier is repeated. Sample P-4 shows a small hump at 393° K. This is followed by sample P-2 in the trend, which exhibits a slightly bigger hump at 418° K. Samples P-5 and P-6 show well defined peaks at 408° K and 413° K respectively. The peaks shift further to 418° K and 423° K for samples P-1 and P-3 respectively. The shift in the temperatures of the peaks looks quite interesting in view of the order that it assumes. More significant is the increase in the intensity of the peaks in the same order. This order is exactly the one that is seen for the performance of these samples. This is supported by the basic fact that better phosphors should use more of the UV radiation for fluorescence rather than for generating defects, which should be to the minimum possible extent. Thus a phosphor in which minimum TSL centres are generated due to the incidence of UV

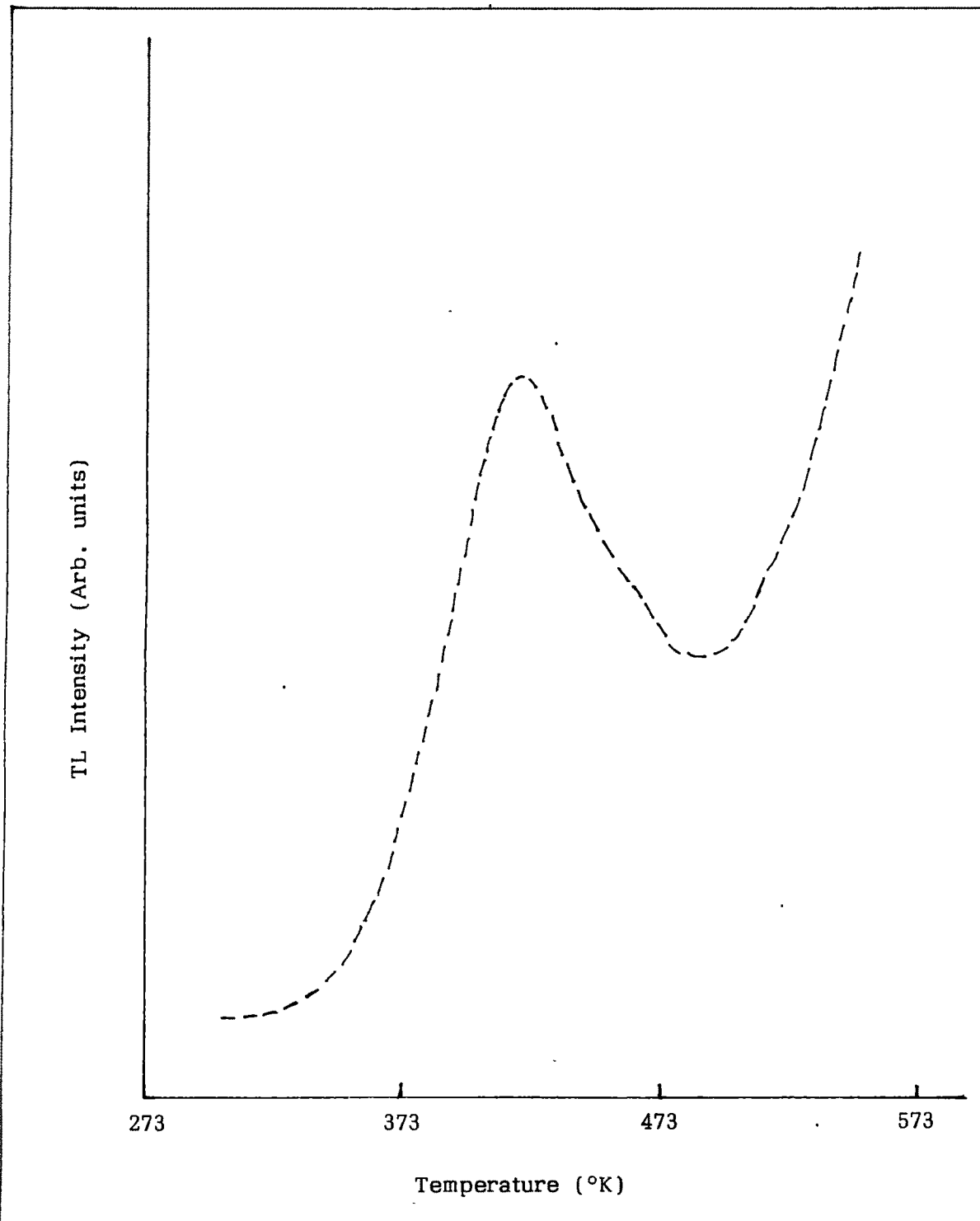


Fig. 3L-I : TSL glow curve (UV irradiated) for sample P-1.

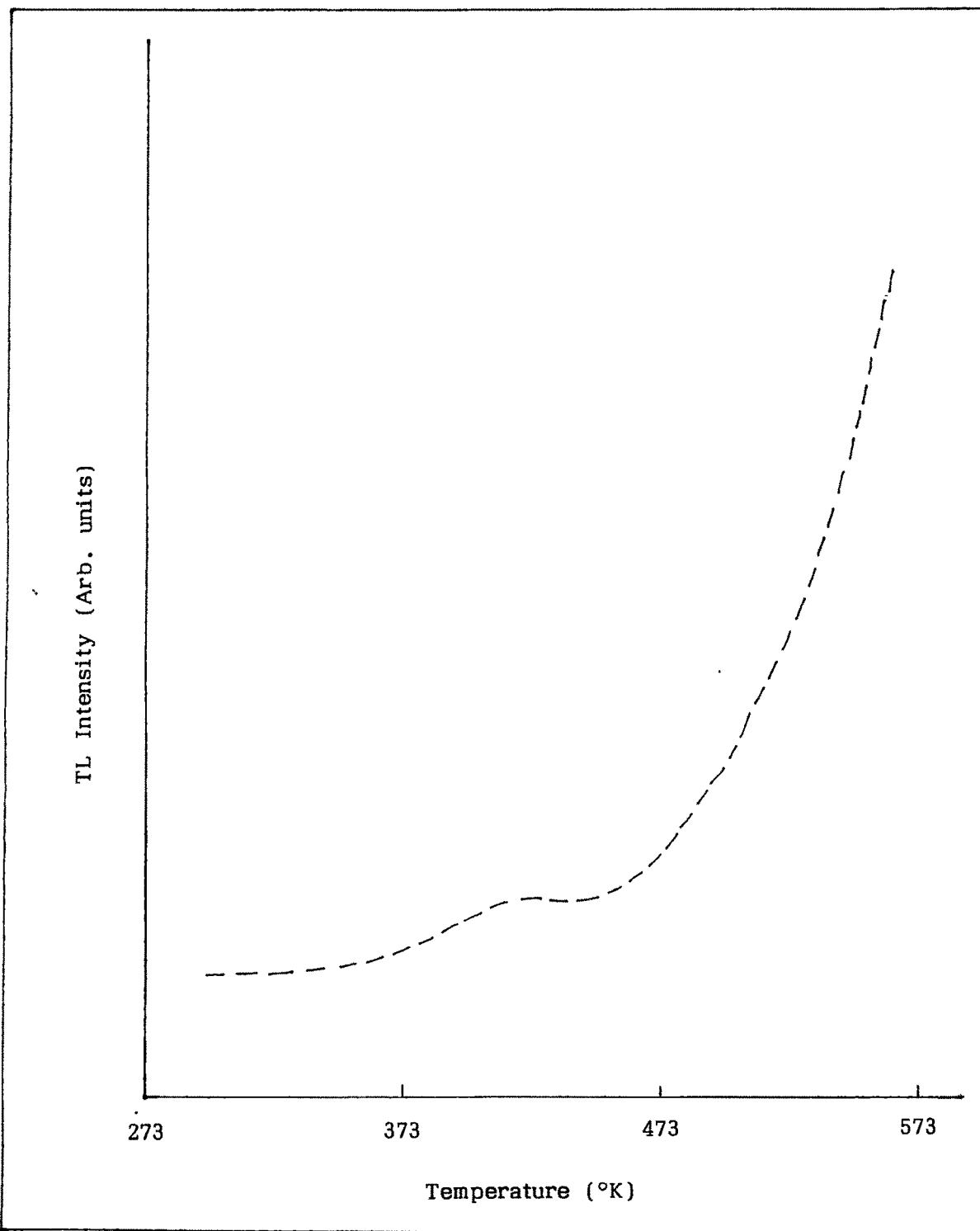


Fig. 3L-II : TSL glow curve (UV irradiated) for sample P-2.

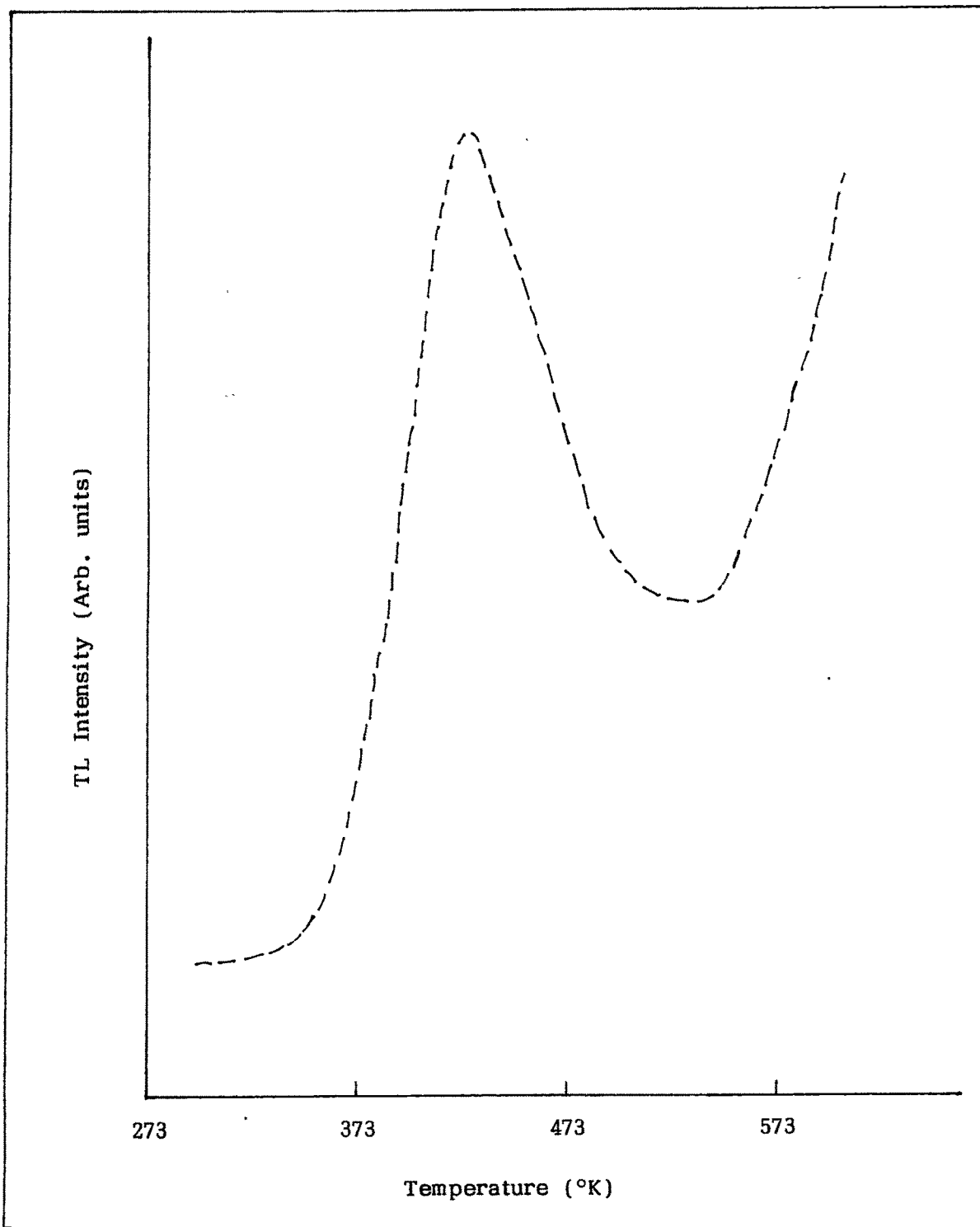


Fig. 3L-III : TSL glow curve (UV irradiated) for sample P-3.

TL Intensity (Arb. units)

273

373

473

573

Temperature ($^{\circ}$ K)

Fig. 3L-IV : TSL glow curve (UV irradiated) for sample P-4.

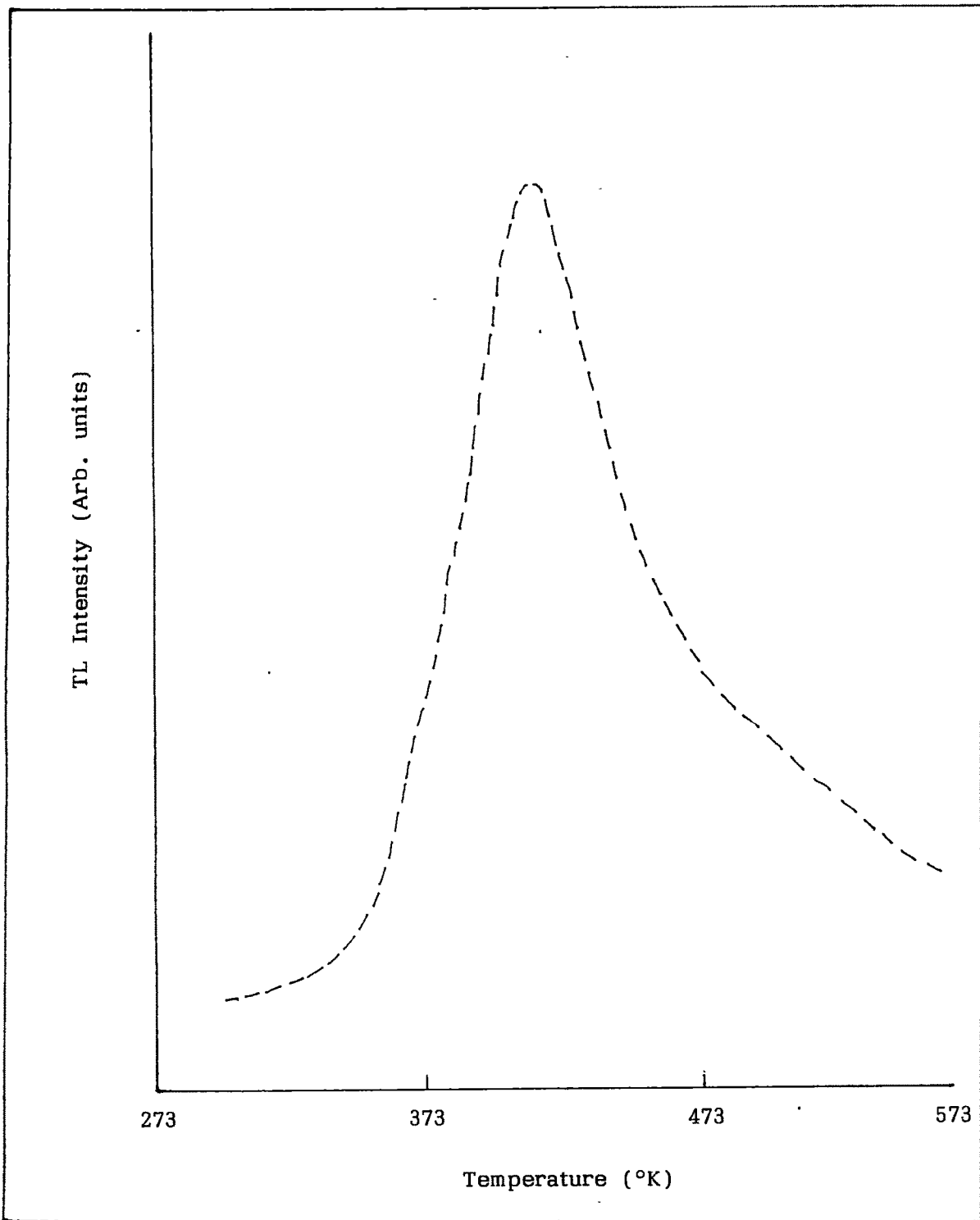


Fig. 3L-V : TSL glow curve (UV irradiated) for sample P-5.

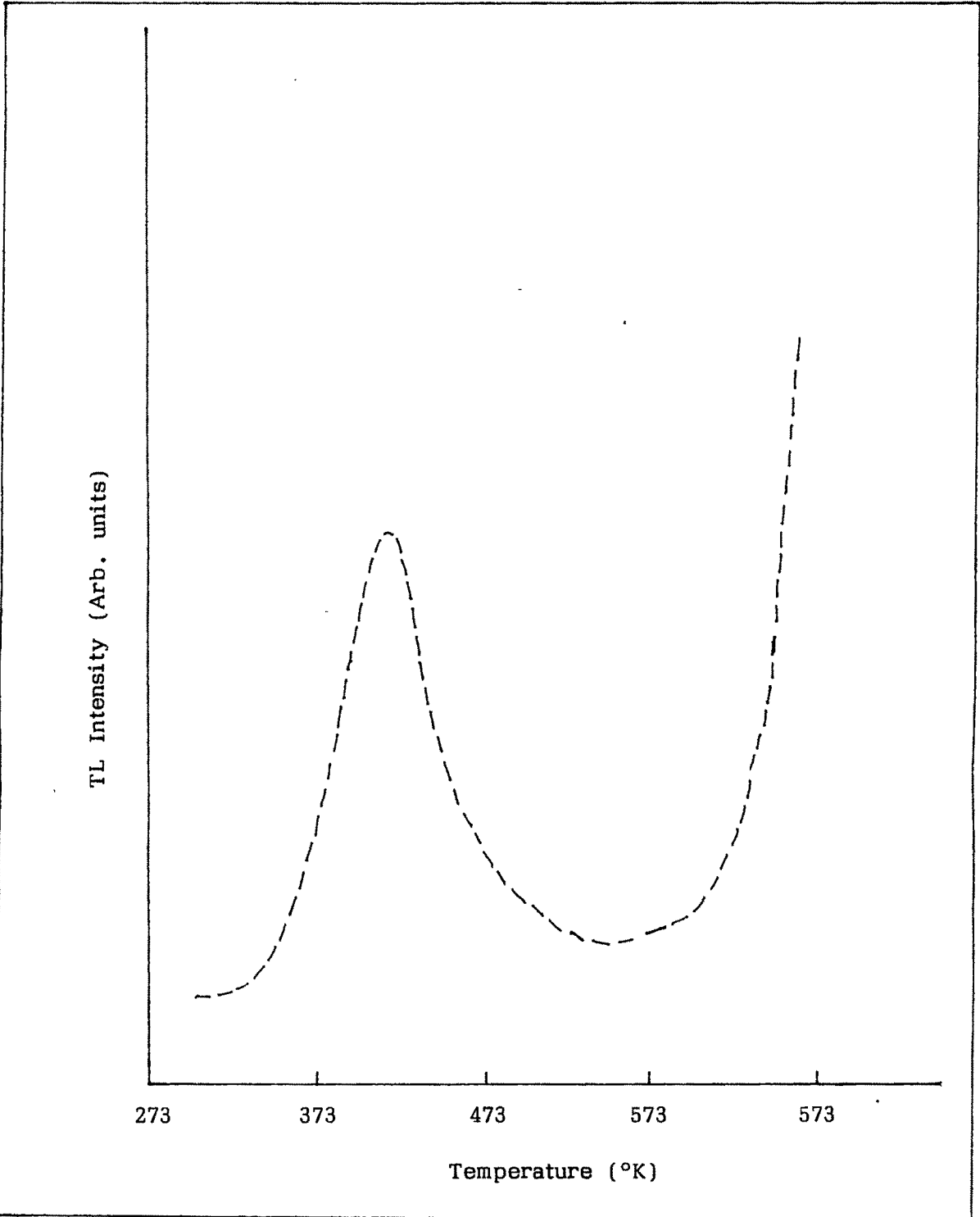


Fig. 3L-VI : TSL glow curve (UV irradiated) for sample P-6.

photons and other radiations as well, is most suitable and hence gives the best performance.

Using the same method, that was used to find the activation energy for gamma irradiated peaks, the activation energy of the UV irradiated peaks were also calculated. The results are given in **Table 3.12**.

Table 3.12 :

<u>Sample</u>	<u>Peak Temp. (° K)</u>	<u>Activation Energy (eV)</u>
P-1	418° K	0.836 eV
*P-2	418° K	0.836 eV
P-3	423° K	0.846 eV
*P-4	393° K	0.786 eV
P-5	408° K	0.816 eV
P-6	413° K	0.826 eV

* only humps.

The peaks correspond to an average activation energy of 0.824 eV, with a variation of 0.06 eV. Looking to the small range of variation, it may be suggested that the same TSL centre is associated with the peaks. The peak temperature variation from 393° K to 423° K is however curious, as the host matrix is the same in all samples. Hence, it may be suggested that the peaks are associated with the aggregation of the impurity ions, i.e. dopants in this case. Lesser the aggregation, lower is the intensity of the peak, and better is the performance expected from the phosphor as less number of energy absorbing, transferring and emitting centres of fluorescence, are converted into TSL traps. More absorption, transfer and emission naturally means better performance.

The TSL intensity being very low in this case, the TSL spectral and EPR investigations could not be carried out in spite of several attempts.

EPR Spectra :

The EPR spectra was taken on a Varian V-4502 EPR spectrometer operating in the X-band range of frequencies (8.8 - 9.5 G.Hz).

Since it was already established that the dopants are Antimony and Manganese, it was expected that the latter i.e. Manganese (atomic number - 25) which is in Mn^{2+} state and is therefore paramagnetic would be giving the signals in the EPR spectra. The expectation was not only proved right but went beyond, in the sense that it completely dominated the spectra and masked any other signal that could be deciphered.

Fig. 3M shows the signals in the EPR spectra due to Mn^{2+} having sextet hyperfine structure with $g = 2.0015$. The second derivative has been presented to make it distinct. DPPH (α , α^1 - diphenyl picryl hydrazyl) with a g value of 2.0036 was used as reference. All the six samples gave similar results. The samples have been generally perceived to be quite stable under irradiation. This is because even a higher dose of γ - radiation could not give any perceptible signals of the defect centres.

The irradiation was carried out at room temperature and the EPR spectra was recorded at the different peak temperatures for each sample. At each of these temperatures, Mn^{2+} signal dominated the spectra.

Corelation :

Manganese is one of the dopants in the investigated samples. As mentioned above, the signal from this dopant masks any signals that come from the TSL centres/defects formed in the host lattice. However this did not become much of a handicap for the study, as a lot of information on the centres, defects in the host lattice i.e. calcium chloro/fluoro apatite, formed due to irradiation, is available. There is a general conclusion, that comes out of the study of TSL - EPR in apatites and it is that the main trapping centres are specific of the crystal lattice [33,34,35,36,37]. Other studies conclude that, no main TSL

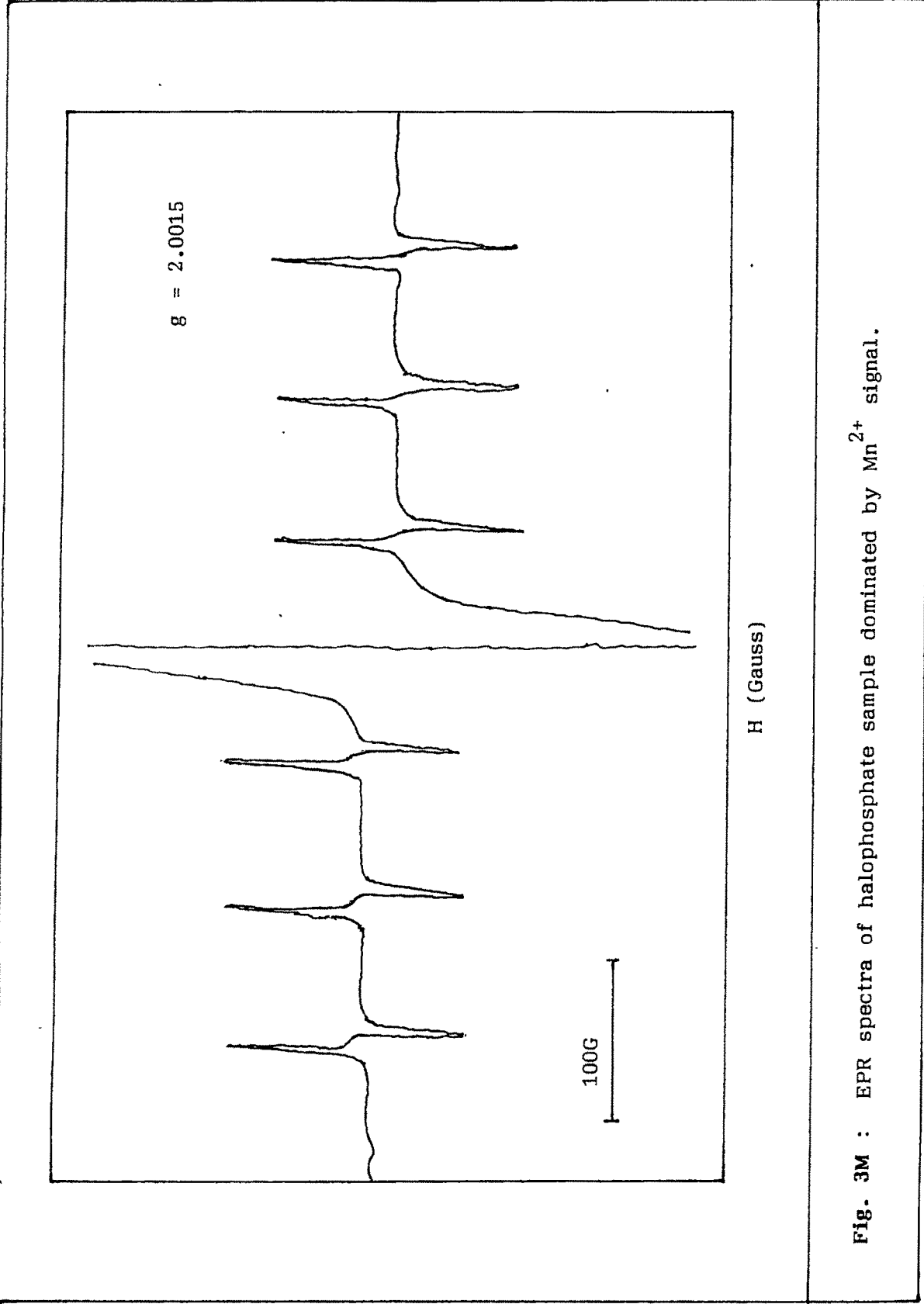


Fig. 3M : EPR spectra of halophosphate sample dominated by Mn^{2+} signal.

peak is connected with the thermal bleaching of the main colour centres or paramagnetic centres which are observed in apatites and which are due essentially to vacancies and O^{2-} defects in halide sites [38,39,40].

The creation of colour may be initiated in several ways [41]. The ionizing radiation removes an electron from the chlorine/fluorine ion resulting in a hole, which is most likely to be transferred to one of the neighbouring phosphate groups. Next, a monovalent ion is disconnected from the PO_4^{3-} group forming together with the chlorine/fluorine ion an $(OCl)^{2-} / (OF)^{2-}$ molecular ion. An alternative possibility is the creation of a hole on a $(PO_4)^{3-}$ ion by removing an electron from this group. The resulting $(PO_4)^{2-}$ radical is not stable and is split into $(PO_3)^{\cdot-}$ and $O^{\cdot-}$, the latter ion together with Cl^- / F^- again forming an $(OCl)^{2-} / (OF)^{2-}$ molecular ion. The electrons produced by both the above processes may be trapped at chlorine/fluorine vacancies, giving rise to F-centres or at more complex defects generally resulting in diamagnetic colour centres

Apart from the PO_4^{3-} , PO_4^{2-} and FO^{2-} / ClO^{2-} radicals, $O^{\cdot-}$, $O_2^{\cdot-}$ and H^{\cdot} have been also reported. The formation of $(ClO)^{2-} / (FO)^{2-}$ and H^{\cdot} radicals depend upon some other factors also viz. conditions maintained during synthesis, moisture absorption etc. EPR work is reported on apatite single crystals grown in air atmosphere and HCl atmosphere [42]. It is believed that crystals grown in air atmosphere are likely to incorporate a small percentage of oxygen impurity ions substitutional for halide ions and the introduction of corresponding charge compensating halide ion vacancies. On the other hand HCl atmosphere yields purer stoichiometric crystals, which give better results in terms of performance also. Hence the number of $(ClO)^{2-} / (FO)^{2-}$ molecular ions will be less in such type of crystals. Thus, it may be considered that the number of $(ClO)^{2-} / (FO)^{2-}$ radicals have a dependence on the quality of crystals to a certain extent

The EPR spectra of X - irradiated oxygen contaminated calcium chloroapatite crystals have been assigned to $(ClO)^{2-}$ molecular ions as it contains $O_2^{\cdot-}$ impurities while in oxygen free crystals, the $(ClO)^{2-}$ centres were completely absent.

The H° atom centres are bound to the OH^- ions, which can be probably present at trace levels in the samples. The OH^- ion is a common impurity known to occur in alkaline earth halides, a raw material used in the preparation of the halophosphate samples

It has been reported that the main radical ion $(ClO)^{2-}$ shows only a partial reduction in intensity and is stable up to $673^\circ K$ [43]. The thermal destruction of the $(ClO)^{2-}$ radical occurs only beyond $673^\circ K$, indicating that it does not play any role in the TSL process below $673^\circ K$. As all the samples in this study were investigated for TSL up to $673^\circ K$ only, the possibility of the role of $(ClO)^{2-}$ molecular ion is ruled out. However the centres H° , O_2^- and PO_4^{2-} seem to be associated with the TSL peaks observed. Of these the H° and O_2^- centres are generally associated with factors that are related to the preparation i.e. they creep in as impurities in the form of oxygen and moisture present in the air. PO_4 group molecular ions are however an integral part of the lattice and are believed to be playing a crucial part in the TSL process [44].

The entire process of TSL involved with the PO_4 group of molecular ions may be proposed as under.

On irradiation, electrons are removed from oxygen atoms of PO_4 groups are trapped very near these groups. During the thermal activation, electrons are ejected out of the trapping centres and transferred by a localized interaction to O^- ions with which recombination is produced. This recombination may take place either non-radiatively, where the lattice emission is re-absorbed by Mn^{2+} ions producing the characteristic greenish yellow emission band or with a transfer of non-radiative energy from oxygen ions to Mn^{2+} ions, again producing the excitation of the latter. This model is supported by the fact that the lattice emission is weakening, when the concentration of Mn^{2+} ions increases, [45] the probability of energy transfer being more important (Fig. 3N).

The above model accounts for the second greenish yellow peak that has been recorded in the TSL spectra of the samples. As per this model, the recombination centre is O^- ion and hence the occurrence of this emission peak may be subject to the availability

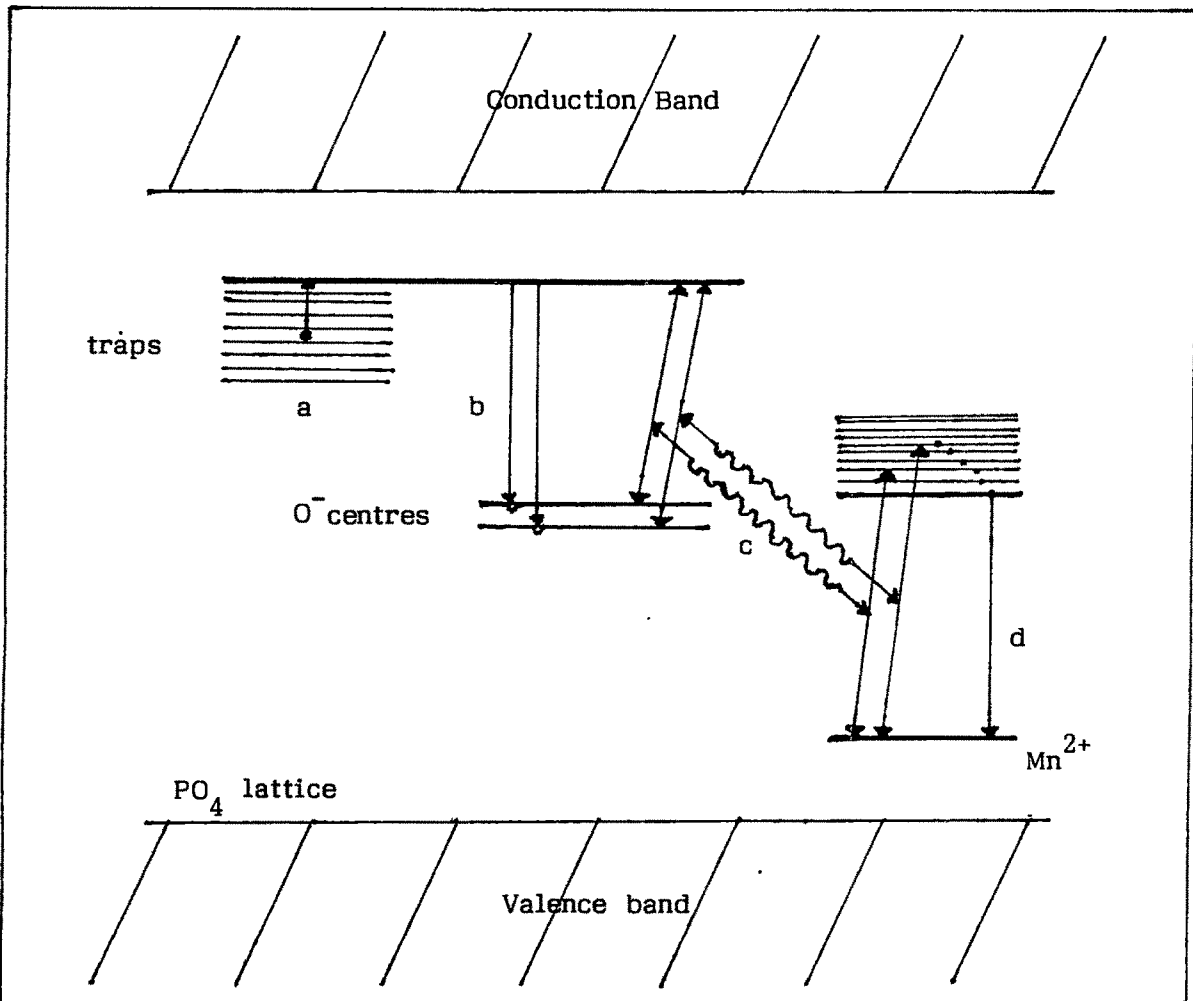


Fig. 3N : Model for TSL mechanism of PO_4 group radicals.

- a - release of electrons.
- b - radiative recombination.
- c - non-radiative transfer to Mn^{2+} ion.
- d - radiative transition.

of oxygen ions, which may get contaminated into the lattice during synthesis. For purer crystals or crystals with lesser degree of oxygen contamination, there might be some effect on this emission peak.

Going back to the TSL spectra of sample P-4, it needs attention that the second emission peak is totally absent for higher temperatures. Hence, it may be concluded that, in this sample, the TSL centres responsible for the second emission peak are present in smaller number and are bleached at a lower temperature. Thus the sample is relatively better in terms of oxygen contamination i.e. it has better purity. It needs to be mentioned again that this same sample has been found to be the best in terms of lamp performance too.

Coming to the discussion of the first emission peak in the TSL spectra, several possibilities can be suggested.

- (a) Energy emitted due to thermal destruction of H° centre is transferred to Mn^{2+} ion causing excitation of the latter.
- (b) Energy emitted due to thermal destruction of H° centre is transferred to Sb^{3+} ion causing excitation of the latter.
- (c) Energy emitted due to thermal destruction of O_2^{2-} centre is transferred to Mn^{2+} ion, causing excitation of the latter
- (d) Energy emitted due to thermal destruction of O_2^{2-} centre is transferred to Sb^{3+} ion causing excitation of the latter.

In these samples, Mn^{2+} is the activator, while Sb^{3+} is the coactivator and sensitiser. Hence excitation of Sb^{3+} ion might lead to transfer of some energy to Mn^{2+} , excitation of which gives rise to the second emission peak while the rest of the energy retained by Sb^{3+} manifests into the first emission peak. As the intensity of the first emission peak increases with temperature, it may be proposed that the probability of transfer of energy from the recombination centre to Sb^{3+} increases with temperature. However, one has to bear in mind that the concentration of Sb^{3+} ions is much less compared to Mn^{2+} ions in

conventional lamp phosphors and hence the probability of energy absorption by Sb^{3+} ions decreases to that extent.

Alternately, it may be proposed that the energy emitted due to the thermal destruction of TSL centres is transferred to Mn^{2+} ions, which undergoes transition between two sets of energy levels and emits a photon corresponding to the wavelength of the first emission peak recorded in the TSL spectra. As per this model, the same activator is responsible for both the peaks. This is possible logically, if the energy absorbed by the Mn^{2+} ions comes from different TSL centres. The same thing is possible again if the Mn^{2+} ions attain different sites in the crystal lattice, which is indeed the case. This model is supported by reports [46].

Going by the above discussion, it may be concluded that,

- the first TSL peak is due to the thermal destruction of the PO_4 group centres
- the second and third TSL peaks are generally due to the thermal destruction of H° and O_2^{2-} centres.
- the first emission peak in the TSL spectra (around 410 nm) can be attributed to the H° and O_2^{2-} centres.
- the second emission peak in the TSL spectra (around 550 nm) can be attributed to the PO_4 group centres.
- the emission can be generally attributed to the Mn^{2+} ion transitions

References :

1. Y. Fukuda, K. Mizugadi, S. Yokota and N. Takenchi, Radiation Protection dosimetry, 70, 93 (1987)
2. Encyclopaedia of Chem. Tech., Vol. 14, 535.
3. M. Kottaiswamy, R. Jagannathan, P. Jeyagopal, R.P. Rao and R.L. Narayanan, J. Phys. D : Appl. Phys., 27 (1994), 2210-2215.
4. Kay M.I., Young R.A and Posner A.S., Nature, 204, (1964), 1050.
5. J.S. Prener, J. Electrochem. Soc., 114(1) (1967), 77.
6. A.H. Hoekstra, Proceedings of the International conference of Luminescence, 1966, (1337-1341).
7. K.H. Butler, Proceedings of the International Conference of Luminescence, 1966 (1313-1329).
8. Bril A. & Hoekstra W, Philips Research Reports, 16(1961), 356
9. Z. Bodo, Acta. Phys. Acad. Sei. Hung., 3, 23, (1953)
10. C.W. Jerome, This Journal, 100, 586 (1953)
11. G.R. Fonda, Brit. J. Appl. Phys. Suppl., 4, 517 (1954).
12. J. Tregellas - Williams, Jour. of Elect. Soc., 105(3), 173, 1958.
13. F.C. Palilla and B.E. O'Rcilly, Jour. of Elec. Soc., 115(10), 1076, 1968.
14. T Forster, Ann. Phys. Leipzig, 2, 55 (1948).
15. D L Dexter, J. Chem Phys., 21, 836 (1953).
16. W Elenbass, Fluorescent Lamps and Lighting, 43, 1959.
17. Kapoor J.K., Thermoluminescence & Its Applications, 18, 1992.
18. J.G. Rabatin, Gillooly G.R. and J.W. Hunter, J of Elec. Soc., 114, 9, 956 (1967).
19. A. Watchtel, J. of Elec. Soc., 113, 2, 128 (1966).
20. Jenkins H.G., *et al.*, This Journal, 96, 1 (1949).

21. Gawford J.H. and L. M. Slifkin, 'Point defects in ionic Solids', Plenum Press, New York, London (1972).
22. Fowler W.B., 'Physics of colour centres', Academic Press, New York (1968).
23. Schulman J. H. and W. D. Compton, 'Colour centres in Solids', McMillan Company, New York (1962).
24. Radhakrishna S. & B. V. R. Chowdhari, Fortshritteder Physik, 25, 511-578 (1977).
25. Itoh N., Cryst. Latt. Def. 3, 115-143 (1972).
26. Groves G. W. & A. Kelley, Phil. Mag. 8, 1437 (1963).
27. Hibi T. & K. Yada, J. Electron Microscopy, 10, 164 (1961).
28. R. de L. Kronig and W. G. Penney, Proc. Roy. Soc. (London) A130, 499 (1930).
29. Bube R. H., 'Electronic properties of crystalline solids', Academic Press, New York (1974), 305-309.
30. Patil P. D, Thesis, M.S. University, Baroda (1996).
31. Sheshagiri T. K, Thesis, Bombay University (1990).
32. Urbach F., Zur Luminescence der alkali halogemide, Wiener Ber. II a, 139, 363 (1930).
33. Lapraz D, Banmer A. and Iacconi P, Phys. Status Solidi, A 54, 605 (1979)
34. Lapraz D, Thesis, University of Nice (1980).
35. Lapraz D, Banmer A, Phys. Status Solidi, A 68, 309 (1981)
36. Fukuda Y, Mijuguchi K, Yokota S and Takenchi N, Radiat. Prot. Dosimetry, 70, 89 (1987).
37. Ceve P, M. Schara, C. Raonik, Radiation research, 51, 581-589 (1972).
38. Piper W.W., L. C. Kravitz, R. K. Swank, Phys. Rev, 138, 1802 (1965).
39. Knotterus D.I.M., Thesis, University of Groningen (1976).

40. Knotterus D. I .M., A. Lanjouw, H. W. Den Hartog, Phys. Stat. Solidi (A), 41, 95 (1977).
41. Knotterus D.I.M., H. W. Dentlartog, Phys. Stat. Solidi (a), 29, 183 (1975).
42. Ronfosse A., M. Staplebroek, R.H. Bartram, O.R. Gilliam, Phys. Rev., 9, 855 (1974).
43. Seshagiri T.K., V. Natrajan, M.D. Sastry, Pramana Joul. of Phys, Vol. 39, No.2, 131-144 (1992).
44. Lapraz D., F. Gamme, M. Barland, Phys. Stat. Sol (a), 59, 249 (1985).
45. Lapraz D. & A. Banmer, Phys. Stat. Solidi, (a), 80, 353 (1983).
46. Meijerink A., G Blasse, J. Phys. : Condens. Matter, 2, 3169 (1990).